

**Master Thesis
in the area of Building Materials**

**Influence of PCE superplasticizers on
ettringite precipitation**

Johannes Lohner

March 22, 2018

Prof. Robert J. Flatt, ETH
Prof. Paulo Monteiro UCB
Dr. Delphine Marchon, UCB

Abstract

To better understand the underlying physio-chemical mechanisms of polycarboxylate ether (PCE) superplasticizer addition in cement, this report investigates the precipitation of ettringite, also referred to as tri-sulfo-aluminate hydrate (A_{Ft}), as one of the first hydration product of cement. Different characterisation methods are used to look at the morphology and crystal structure of this material. For this reason relatively pure ettringite with and without PCE is synthesized either directly from an aluminium sulphate source ($Al_2(SO_4)_3 \cdot 18H_2O$) and calcium oxide (CaO) or from a C_3A and hemihydrate reaction. From SEM images, strong influence of PCE can be observed on the morphology and the aspect ratio of the crystals. Moreover, BET gas adsorption measurements show a linear increase of the specific surface area (SSA) with PCE dosage. Furthermore, Raman spectroscopy measurements were carried out to investigate the effect of PCEs on the crystal structure of ettringite. Summarizing, hypothesis on the impact of PCEs on A_{Ft} nucleation and growth are made and the influence of the heterogeneity of the solution is discussed.

Eigenständigkeitserklärung

Hiermit erkläre ich, die vorliegende Arbeit selbständig und in eigenen Worten verfasst zu haben. Davon ausgenommen sind sprachliche und inhaltliche Korrekturvorschläge durch die Betreuer und Betreuerinnen der Arbeit.

Ich bestätige mit meiner Unterschrift, das ich

- auf wirkliche und dem Sinne nach der Literatur und Quellen entnommene Gedanken und Ergebnisse verwiesen habe,
- alle Methoden, Daten und Arbeitsabläufe wahrheitsgetreu dokumentiert habe,
- keine Daten manipuliert habe und
- alle Personen erwähnt habe, welche die Arbeit wesentlich unterstützt haben.

I hereby confirm that I am the sole author of the written work here enclosed and that I have compiled it in my own words. Parts excepted are corrections of form and content by the supervisor.

With my signature I confirm that

- *I have committed none of the forms of plagiarism described in the ‘Citation etiquette’ information sheet.*
- *I have documented all methods, data and processes truthfully.*
- *I have mentioned all persons who were significant facilitators of the work.*
- *alle Personen erwähnt habe, welche die Arbeit wesentlich unterstützt haben.*

I am aware that the work may be screened electronically for plagiarism.

Ort, Datum

Unterschrift

Acknowledgement

I want to thank Prof. R.J. Flatt from the institute of building materials at ETH Zurich, CH as well as Prof. Paulo J.M. Monteiro from civil engineering department at UC Berkeley, CA that made this work possible. Moreover, without the help of David Gardner, who consulted me and helped me with the Raman spectroscopy measurements, Tim Teague, with the support for the XRD and SEM measurements as well as Jiaqi Li, the results of this report wouldn't have been possible. At last, but definitely not least, very special thanks to Dr D. Marchon, who was not only an amazing supervisor, but also an incredible support and teacher.

Abreviations

Table 0.1: Cement chemist notations

C	Calcium	CaO
A	Aluminate	Al_2O_3
S	Silicate	SiO_2
F	Ferrite	Fe_2O_3
\$	Sulfate	SO_3
AFt	Alumina - Ferric Oxide - Trisulfate	$Ca_6Al_2(OH)_12(SO_4)_326H_2O$
AFm	Alumina - Ferric Oxide - Monosulfate	<i>different types</i>
C\$H_2	Gypsum	$CaSO_42H_2O$
CH	Calium Hydroxide (Portlandite)	$Ca(OH)_2$
C-S-H	Calicum Silicate Hydrate	$xCaO \cdot ySiO_2 \cdot zH_2O$
C ₃ S	Tricalcium Silicate	Alite
C ₂ S	Dicalcium Silicate	Belite
C ₃ A	Tricalcium Aluminate	
C ₄ AF	Tetracalcium Aluminoferrite	

Table 0.2: Acronyms

OPC	Ordinary Portland cement
PCE	Polycarboxylate ether
FBW	Flexible backbone worm
SC	Side chain
PEG	Polyethylen glycol
PMA	Polymethacrylic acid
C/E	Carboxylate to ester ratio
P	Side chain length
N	Number of monomers in backbone for one SC
n	Number of repeat units in one molecule
TGA	Thermogravimetric analysis
XRD	X-Ray diffraction
SEM	Scanning electron microscope
SSA	Specific Surface Area

Contents

Abstract	I
1 Introduction	1
2 Theoretical Background	3
2.1 Cement hydration	3
2.2 Ettringite	5
2.2.1 Ettringite molecular structure	5
2.2.3 Polycarboxylate ether (PCE)	7
2.3.1 Structure of PCE	7
2.4 Influence of PCE during ettringite precipitation	10
2.4.1 Ettringite from C_3A reaction	10
2.4.2 Ettringite from direct synthesis	11
2.5 Influence of PCE during cement hydration	12
3 Material and Methods	15
3.1 Synthesis of ettringite	15
3.1.1 Mixing	15
3.1.2 Filtering	17
3.1.3 Drying	17
3.2 Characterisation methods	18
3.2.1 Powder X-Ray Diffraction	18
3.2.2 Scanning Electron Microscope (SEM)	19
3.2.3 BET gas adsorption	20
3.2.4 Thermogravimetric analysis	20
3.2.5 Raman spectroscopy	21
4 Results	23
4.1 Filtering	23
4.2 X-Ray Diffraction	23
4.3 TGA	25
4.4 Morphology analysis	26
4.4.1 Ettringite from direct synthesis	26
4.4.2 Ettringite from reaction of C_3A and hemihydrate	30
4.5 BET gas adsorption	33
4.6 Raman spectroscopy	36
4.6.1 Deconvolution of PCE Peaks in Raman shifts of AFt+PCE	38
5 Discussion	41
5.1 Morphology and formation of ettringite crystals	41
5.1.1 Nucleation	41
5.1.2 Growth	42
5.1.3 Heterogeneity	43

5.2 Influence of the PCE molecular structure on ettringite formation	44
5.3 Crystal structure of ettringite	44
6 Conclusion	45
7 Outlook	47
A Sample specifications	57
B External Standard	59

1 Introduction

Nowadays, innovation in the construction industry leads to high requirements for the rheological behaviour of concrete and rate of hydration for cement. This usually implies the use of different chemical admixtures to modify and target properties of concrete in the fresh state as well as in the hardened state. Among the most used chemical admixtures, superplasticizers, enable concrete to have good workability as well as high strength and durability. They allow to reduce the water content of concrete without impacting the fluidity of the system. Reducing water leads to lower porosity in concrete and therefore better mechanical strength and resistance against ions ingress ([Aïtcin & Flatt \(2015\)](#)). However, it has been found that superplasticizers (SPs) present significant drawbacks, such as retarding cement hydration, which leads to less early strength development ([Marchon et al. \(2017\)](#)). This problem occurs, because SPs act on the complex system of cement hydration. Cement hydration involves three different mechanisms, that are dissolution, nucleation and growth of various phases reacting at different time and speed.

One of the most reactive phase in anhydrous cement is tricalcium aluminate C_3A . When dissolved in water calcium aluminate hydrate phases (CAH) precipitate that lead to a general stiffening of cement paste without sufficient strength development (flash set). To prevent this negative effect, gypsum is added into the system that reacts with the tricalcium aluminate to form ettringite ([Mehta & Monteiro \(1976\)](#)).

In this study, the focus is set on the influence of polycarboxylate ester (PCE) on the precipitation of ettringite. The interaction of those two components, are known to lead to less effectiveness or even incompatibility of some PCEs in concrete. A strong influence of PCE on nucleation and growth of ettringite could lead to an unbalanced system ([Aïtcin & Flatt \(2015\)](#)). The result, a decreased workability and strength development.

Ettringite is an already well known compound ([Goetz-Neunhoeffer et al. \(2006\)](#), [Moore & Taylor \(1970\)](#), [Cody et al. \(2004\)](#), [Barger et al. \(2001\)](#), [Goto et al. \(1995\)](#), [Black et al. \(2006\)](#), [Hartman & Berliner \(2006\)](#)). Better controlled superplasticizers have been developed and analysed ([Gelardi & Flatt \(2015\)](#), [Gelardi et al. \(2015\)](#), [Wiliński et al. \(2016\)](#), [Marchon et al. \(2016\)](#)) and the influence of them on ettringite have been made [Meier et al. \(2016\)](#), [Meier & Plank \(2016\)](#), [Dalas et al. \(2015\)](#), [Cody et al. \(2004\)](#). Despite all this work, still many open questions, like what effect PCEs have on nucleation, growth and crystal structure of early hydration products, remain ([Gelardi et al. \(2015\)](#)).

The main objective of this work is therefore to study the effect of PCEs on ettringite precipitation. A focus is done on the change of morphology (SEM), specific surface area (BET gas adsorption) and crystal structure (Raman spectroscopy).

2 Theoretical Background

2.1 Cement hydration

The underlying chemical hydration processes that determine cement hydration are:

- Dissolution

Takes place when a material is put into solution where the ion concentration is lower than what it would be at the equilibrium. C_3A has a very high solubility and dissolves fast when getting in contact with water. Dissolution will happen until a saturated solution with respect to a phase is reached.

- Supersaturation

Will occur, when too much ions are present in the solution. This results in a crystal growth that again leads to a solution in equilibrium. Since the saturation equilibrium for hydrates is lower than for anhydrous phases, crystals are growing, before a supersaturation with respect to anhydrous phases is reached.

- Nucleation

This is the initial formation of a hydrate in a supersaturated solution. It is a complex process that today is still not understood. It doesn't occur immediately and depends on the formation of so called nuclei in a high ion concentration. The nuclei form and dissolve until they reach a certain critical size that allows them to further grow.

- Growth

Growth of crystals in the supersaturation.

In cement chemistry a simplified notation of the minerals, that does not include small impurities of magnesium, sodium, potassium or sulphur in the minerals and can be seen in table 0.1 is used. Anhydrous ordinary portland cement (OPC) consists of the anhydrous clinker phases C_3S (65%), C_2S (15%), C_3A (7%) and C_4AF (8%) as well as of usually 5% gypsum. In contact with water those phases react and precipitate the four main hydration products C-S-H, CH, AFm and Aft. Thereby particularly C-S-H (no strict ratio of of SiO_2 to CaO) but also CH coming from C_3S and C_2S hydration are responsible for the long term strength. The two most common AFm and Aft phases are ettringite (15-20%, from [Barger et al. \(2001\)](#)) respectively monosulphate. The hydrated cement consists of 60-70% silicate and 10-20% aluminate hydrates. As the total chemical reactions during cement hydration are exothermic they can be represented by a calorimetric curve, shown in figure 2.1.

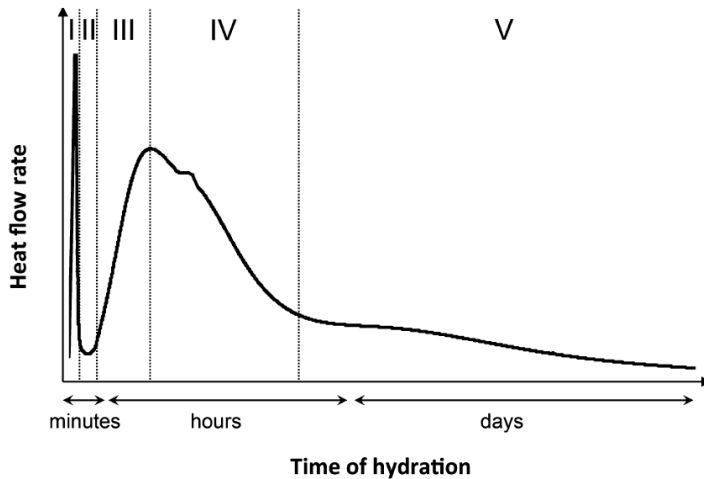


Figure 2.1: Calorimetric curve of cement hydration from Marchon & Flatt (2016)

This curve is also often referred to as the chemical footprint of cement hydration and can be divided into five different stages.

In the first stage, which is called "initial dissolution", the contact of cement with water results in a strong exothermic reaction. The most reactive clinker phase is tricalcium aluminate (C_3A), which dissolves faster than C_3S , C_2S and C_4AF . The released oxide ions and the presence of alkalis lead to a high amount of OH^- ions and therefore to a high pH solution between 12 to 13. During this process C_3S and C_2S get surrounded by gradients of ionic concentration that reduces their dissolution. As mentioned in Lasaga & Lutz (2001), the rate of dissolution is strongest at high undersaturation, in the beginning of the dissolution, and decreases as the saturation of the solution reaches equilibrium. It could be found that besides intensive mixing, corners or imperfections like inclusions and etch pits on the surface of anhydrous phases enhances their dissolution. The same effect appears for finely ground anhydrous cement.

The strong heat release is soon followed by a sudden slowdown in reaction and the start of the induction period (stage II in figure 2.1), which marks a time of slow reaction. One possibility for this slow reaction could be that no nucleation of silicate hydrates has set in. Garrault et al. (2006) could show that calcium silicate hydrate (C-S-H) and portlandite (CH) already nucleate during this time, which supports another theory that suggests that a decreasing dissolution rate of anhydrous phases is matched by an increasing growth rate of hydrates.

Once a critical oversaturation of the solution has been reached, a fast increase of silicate precipitation takes place. This leads to the acceleration period (stage III in figure 2.1) which is important as C-S-H is most responsible for long term strength. The hydration rate is decreasing as more space is taken by hydration products. The heat release curve in figure 2.1 reaches a peak (sometimes called silicate peak) which corresponds to the highest rate of reaction.

Afterwards, the deceleration period IV starts. There the hydration rate decreases as more and more space is occupied by the hydration products. As a result of the depletion of the sulphate source, the sulphate depletion point (or aluminate peak) occurs. This can be seen as a small shoulder in stage IV. At this point all sulphate ions are dissolved which leads to a faster reaction. In this stage, the hydration is slow and driven by the diffusion of ions.

in the hardened paste. The aluminates in the solution increase again due to the renewed hydration of C_3A and C_4AF [Mehta & Monteiro \(1976\)](#).

While no more ettringite can be formed, the already hydrated ettringite in the system becomes unstable and transforms to the more stable monosulphoaluminate (AFm) phase by reacting with the remaining C_3A . This results in another broad but low peak in the steady state stage V.

Influence of sulphates in cement hydration

Without the right amount of sulphates, that come from the addition of gypsum in cement, the dissolved and highly reactive calcium oxide and aluminate ions would form different amounts of calcium aluminate hydrates (CAH). Both, the favoured precipitation of CAH on the surface of C_3S and C_2S as well as the higher concentration of aluminium ions that could adsorb on the anhydrous silicate particles, inhibit the dissolution of C_3S and C_2S [Pustovgar et al. \(2017\)](#). Thereby CAH not only leads to stiff and unworkable concrete but also reduces silicate hydration and long term strength development. Especially the latter is the reason why this process is commonly referred to as flash set.

As a solution sulphates are added into the system and ettringite is formed instead of CAH. This is important, as it gives C_3S and C_2S enough time to hydrate. If the sulphate content is too high, however, gypsum needles could lead to weak concrete properties (false set). Therefore usually an amount of 5-6% gypsum is added in OPC.

2.2 Ettringite

Ettringite is an alumina ferric oxide trisulphate (AFt) also referred to as trisulfoaluminate hydrate or trisulphoaluminateferrite hydrate ($3CaO \cdot Al_2O_3 \cdot 3CaSO_4 \cdot 32H_2O$). AFt thereby is often used as synonym for ettringite, which is also done in this work. The stoichiometric reaction that leads to the precipitation of ettringite during cement hydration can be seen in equation 2.1.



The highly reactive aluminate and calcium ions from C_3A and low solubility of ettringite in the alkaline solution leads to the almost immediate precipitation of ettringite ([Meier et al. \(2016\)](#) observed nano-sized ettringite crystals after 10 seconds of hydration). AFt formation thereby plays an important role for the balance of the hydrated cement phases (C_3S , C_2S , C_3A , C_4AF) in the system. Furthermore ettringite leads to stiffening (loss of consistency), setting (solidification of the paste) and early strength development of cement ([Mehta & Monteiro \(1976\)](#)).

2.2.1 Ettringite molecular structure

Ettringite appears in cement in the form of hexagonal needles. The morphology of ettringite can show different sizes and shapes depending on the environmental conditions, such as

solution concentration and pH (Goetz-Neunhoeffer et al. (2006), Moore & Taylor (1970), Cody et al. (2004)). The aspect ratio can have a range of 2.5 to 20. A lower pH and solution concentration leads to longer ettringite crystals with a bigger aspect ratio. Investigating the crystallographic structure, Moore & Taylor (1970) and Brittain et al. (1968) found that ettringite has a trigonal $P31c$ space group. This was later confirmed by Raman study Renaudin et al. (2007) as well as the neutron powder diffraction technique Hartman & Berliner (2006).

Figure 2.2 shows the crystal structure of ettringite, which can be divided into an intra- and an inter-columnar region. The column along the c -axis of ettringite can be seen in figure 2.2b. There the $Al(OH)_6$ octahedra (green) that are surrounded from two sides by three calcium atoms in the form of $Ca(OH)_4(H_2O)_4$ polyhedron (pink), can be seen. Figure 2.2a shows a cross section of the columns along the $a - b$ plane. Moore & Taylor (1970) could show that "the aluminium atoms are six-fold coordinated with hydroxyls and the calcium atoms are eight-fold coordinated with four hydroxyls and four water molecules. The inter-columnar region consist of sulphate anions which are shown in yellow in figure 2.2b and 2.2a. The oxygen atoms of the SO_4^{4-} ions are thereby each connected to twelve hydrogen atoms. In figure 2.2b and 2.2a, several hydrogen (long and green) and O-H bonds (shorter and blue) can be seen. Renaudin et al. (2007) investigated those hydrogen bonds with the help of Raman spectroscopy. The intra-columnar region of the $[Ca_3Al(OH)_6(H_2O)_{12}]^{3+}$ - columns is bond together by hydroxyl groups but also a few linked water molecules ($\frac{1}{8}$ wt %). The cohesion of the inter-columnar region arises from the free water molecules and the rest of the linked water molecules ($\frac{7}{8}$) through the sulphate anions. The large amount of water ($32 \cdot H_2O$) plays an important role in the ettringite structure.

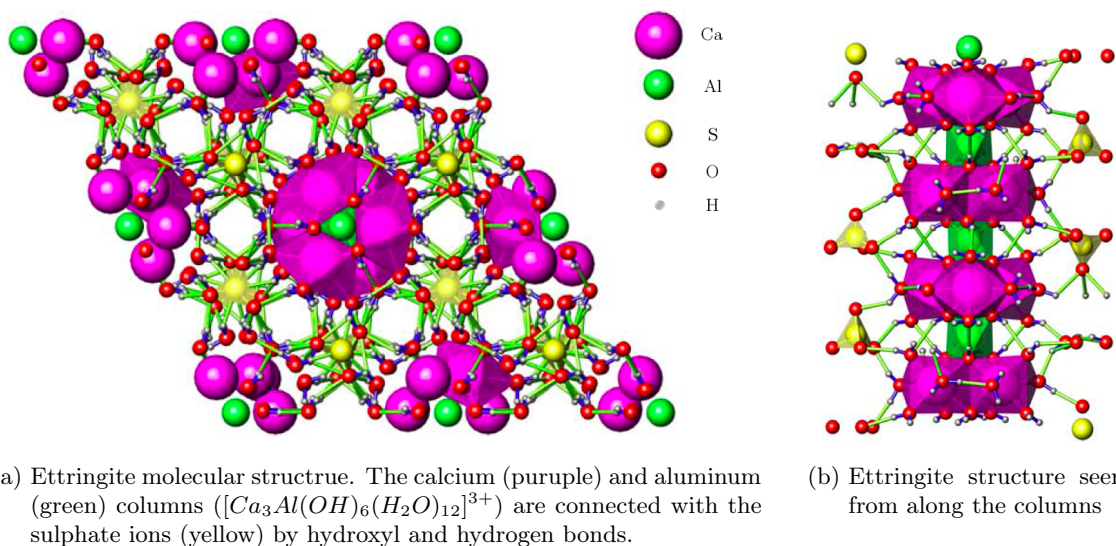


Figure 2.2: The ettringite crystal structure taken and adapted from Hartman & Berliner (2006)

2.3 Polycarboxylate ether (PCE)

PCEs, also called comb-shaped copolymers, are a new generation of superplasticizers (SP) on the market. Superplasticizers or high range water reducers (HRWR) are surface active substances that modify the way particles interact with each other. Because of their high effectiveness and easy modification, PCEs had an increasing popularity in the last decade. For complete hydration, OPC only requires a low w/c ratio of 0.22 to 0.25. However, in order to achieve a reasonable workability, a w/c ratio of more than 0.45 is generally used in normal cement [Mehta & Monteiro \(1976\)](#). PCEs are used to reduce the amount of water and thereby maintaining or decreasing the yield stress and durability of freshly mixed cement. The efficiency of PCEs are unquestioned. [Wiliński et al. \(2016\)](#) could show, that an addition of less than 0.3 wt % of solid content is sufficient to reach a water reduction of 40%. As a result, the use of PCEs allows to reduce porosity and increase durability [Huang et al. \(2016\)](#). Moreover, investigation on the influence of PCEs could show that after 28 days an increase of 30% in compressive strength can be reached ([Li et al. \(2014\)](#), [Wu et al. \(2007\)](#)). The application of PCE, however, is somewhat tricky. The effect of the PCE depends not only strongly on the dosage, their molecular structure and architecture but also on the cement mix, which can vary strongly between batches and is difficult to control. Furthermore, as shown in [Marchon \(2016\)](#), [Zhang et al. \(2015\)](#), PCEs can lead to a high retardation (~ 10 hours) of the acceleration period (stage III in figure 2.1) and therefore a reduction of the early strength. Both are crucial for construction projects as transportation and time pressure require reliable information for the hydration process and rapid strength development. The therefore additional added chemical admixtures in the mix design like accelerators, increase the complexity and price of the cement. As a result the use of PCEs is sometimes, if not often, limited. The physio-chemical mechanisms and influence of PCEs on the microstructure of hydrating cement must therefore be better understood.

2.3.1 Structure of PCE

Figure 2.3 schematically represents the structure of a polycarboxylate ether molecule. It consists of a large molecule composed of many repeat units, each containing one non-ionic hydrophilic side chain (yellow in figure 2.3). The side chains are connected to a long negatively charged backbone (blue in figure 2.3). The backbone (BB) is made up of chains of carboxylate groups (COO^-) that, with their negative charge, lead to dissociation in water and to the adsorption of the SP on positively charged ions. The BB includes functional groups that connect them to the side chains.

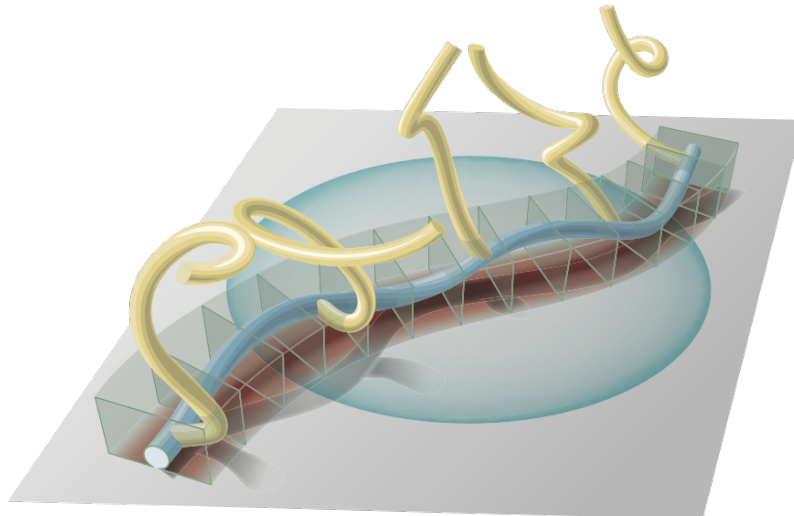
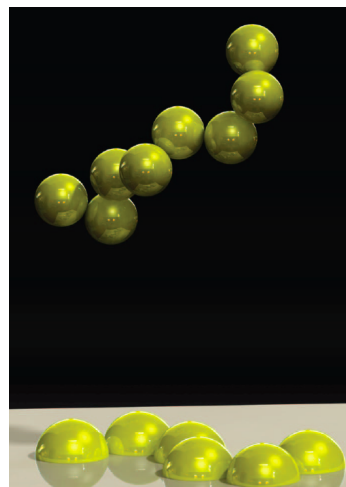


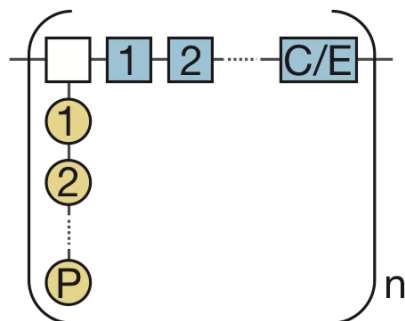
Figure 2.3: Representation of a PCE from Marchon et al. (2017). In blue, the long negatively charged backbone, with hydrophilic yellow side chains

PCEs can have different confirmation of side chains and backbones. The so called flexible backbone worm (FBW), which is used in this report and can be seen in figure 2.4a, is one of five possible arrangements that were first described by Gay & Raphaël (2001). This conformation of the PCE is seen as a long chain of bubbles or cores in solution and as hemi-spheres in the adsorption state.

In Flatt et al. (2009) and Marchon et al. (2017) it is shown how the radius of gyration R (see equation 2.2) as well as the surface occupied by each molecule S_{AC} (see equation 2.3) is calculated. Their size can be directly related to the adsorption efficiency of a PCE.



(a) Representation of a FBW taken from Flatt et al. (2009). It is arranged as a long chain of cores.



(b) Simplified representation of a comp copolymer taken from Marchon et al. (2017).

Figure 2.4: On the left, the confirmation of a FBW and on the right the representation of the structural parameters of a PCE repeat unit

$$R = \left(\left(\frac{a_N}{a_P} \right)^2 \frac{(1 - 2\chi)}{2} \right)^{\frac{1}{5}} a_P P^{\frac{2}{5}} N^{\frac{1}{5}} n^{\frac{3}{5}} \quad (2.2)$$

$$S_A = \left(2\sqrt{2}(1 - 2\chi) \frac{a_N}{a_P} \right)^{\frac{1}{5}} a_P P^{\frac{7}{10}} N^{-\frac{1}{10}} \quad (2.3)$$

Where a_N and a_P is the size of the monomer in the backbone and the side chain (for methacrylic backbones $a_N = 0.25\text{nm}$ and $a_P = 0.36\text{nm}$). χ is the Flory parameter which for poly(acrylamide) as solvent in water is 0.37. The parameters can be seen in figure 2.4b. P is the number of monomers in the SC, N the number of monomers in the backbone for one repeat unit and n the amount of repeat units. $N \cdot n$ is therefore the total number of monomers in the BB for one molecule. $C/E = N-1$ represents the number of free monomers in the BB for one repeat unit. By varying those parameters PCEs can be produced with different adsorption and dispersion behaviours. This effect has been described in further detail by [Gelardi et al. \(2015\)](#) and [Marchon et al. \(2017\)](#). It could be shown that if the ratio of C/E rises (more charged functions in one repeat unit), the charge density and therefore also the adsorption efficiency rises. A higher adsorption efficiency and an adequate side chain length leads to a better dispersive effect and therefore more effective PCEs. Another way PCEs can differ from each other is in the chemical nature of the monomers. The anchor for the side chain on the backbone can for instance be an ester, an ether or an amide group. For the chemical nature of the backbone acrylic or methacrylic functional groups (H or CH_3) are mostly used. But also the chemical nature of the side chains can be changed (PEG, polypropylene oxide etc.). Further detail like advantages and disadvantages of the different functional groups as well as approaches on how to produce PCEs can be read in [Gelardi et al. \(2015\)](#).

How PCE work

The BB of a PCE adsorbs on a particles surface using Van der Waals (VdW) and electrostatic forces. VdW forces use the fluctuations in the polarization of molecules and thereby lead to an attraction over a very short range of less than 0.4nm . Electrostatic forces arise from the negative charge of the carboxylate group in the alkaline solution. It has a wider range and leads to an attraction of positively charged ions and molecules ([Christenson \(1984\)](#)).

The non-ionic SCs of the adsorbed PCEs lead to steric hindrance, which prevents particles from coming to close to each other. Adsorbed PCEs thereby cause repulsion of particles at a distance of 500nm , which without PCE would be 5nm (from [Gelardi & Flatt \(2015\)](#)). During the dynamic process of cement hydration this process is disturbed by the hydration products which limit the effectiveness of the PCEs [Mehta & Monteiro \(1976\)](#).

2.4 Influence of PCE during ettringite precipitation

2.4.1 Ettringite from C_3A reaction

Different theories exist on the influence of PCE on C_3A hydration. Roessler et al. (2007) mentioned a slow down or hindering of the sulphate dissolution due to PCE adsorption. Furthermore a better dispersion of anhydrous phases leading to faster sulphate consumption and ettringite formation was proposed Jansen et al. (2012).

However, since it is known that ettringite formation starts in the first seconds, another theory suggest that this increase in ettringite formation comes from an enhanced nucleation of AFt crystals Comparet (2004). Furthermore Roessler et al. (2007) and Eusebio et al. (2013) remarked that PCE could change the morphology of AFt by affecting the crystal growth.

Yamada (1992) and Zingg et al. (2008b) studied early products of cement hydration by using high pressure freezing with cryo-FIB and cryo-SEM techniques. At the presence of PCE, they noticed hexagonal and short prismatic crystals sub-micron particles in the interstitial pore space. Those crystals were 100 to 500 nm of long ettringite crystals with a variable thickness. The same observation was done by Comparet et al. (2007) and Comparet (2004). This findings indicate an increase in SSA and a decrease in size of precipitated ettringite particles during the first minutes. Moreover it was found that when adding PCE, ettringite crystals passed through the $0.3 \mu m$ filter paper, that wouldn't pass through without PCEs.

Dalas et al. (2015) looked at the hydration of ettringite from a system with 16% C_3A , 4% Calcium Sulphate and 80% Calcium Carbonate. It could be shown that after 5 minutes of hydration the SSA of ettringite can be 6 times higher when 0.15 % PCE is added into the solution. Furthermore Differential scanning calorimetry (DSC) showed that PCE addition results in the precipitation of around one third of all ettringite crystals during the first 30 minutes. Afterwards a reduced rate of reaction was observed as well as a reduction of the total amount of ettringite after 2 hours Dalas et al. (2015). It has also been observed that the specific surface is increased by PCEs addition and that it is decreasing after 5 minutes of hydration. Following hypothesis were considered :

- PCE adsorb on clinker surfaces, making heterogeneous nucleation less favourable (Dalas et al. (2015)).
- PCE lead to homogeneous nucleation by complexing ions and/ or reducing ettringite surface energy (Dalas et al. (2015)).
- PCE strongly interacts with AFt crystal by slowing down or preventing growth. Nucleation is favoured over growth. This theory is consistent with the higher absorption values that have been found for ettringite that precipitation with PCE. PCE may preferentially adsorb on the ettringite surface with high energy ?.
- Small ettringite crystals do not aggregate and do not attach on clinker surfaces because of the repulsive interaction with PCE Zingg et al. (2008b), Zingg et al. (2008a).

The influence of PCE on the SSA of ettringite, reported by Dalas et al. (2015), can be

seen in figure 2.5. The PCE specifications of C20s and C38s can be seen in table 2.1. After 5 minutes a strong increase in SSA was observed. This effect was also reported by Regnaud et al. (2011) and occurs especially for higher dosage and charge density of PCEs. Furthermore the SSA of the samples decreases slightly after 2 hours if a significant amount of PCE was added into the system.

Table 2.1: Specification of C20s and C38s superplasticizer

	C/E	P	MPEG Mw [$\frac{g}{mol}$]
C20s	5	25	1100
C38s	2.6	25	1100

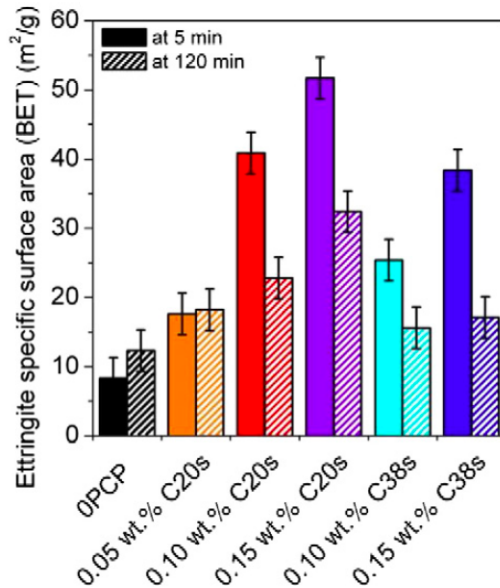


Figure 2.5: SSA after 5 and 120 minutes by addition of different amount of PCE from Dalas et al. (2015)

HOLZER et al. (2007), Zingg et al. (2008b) used cryo-FIB and cryo-SEM techniques to study early cement hydrate products. They found 100 to 500 nm long dispersed ettringite crystals in the pore space and noticed a more particle-free surface of the anhydrous clinker when PCE was added. In the case without PCEs, they also observed small ettringite particles, but this time attached to the surface of the anhydrous clinker.

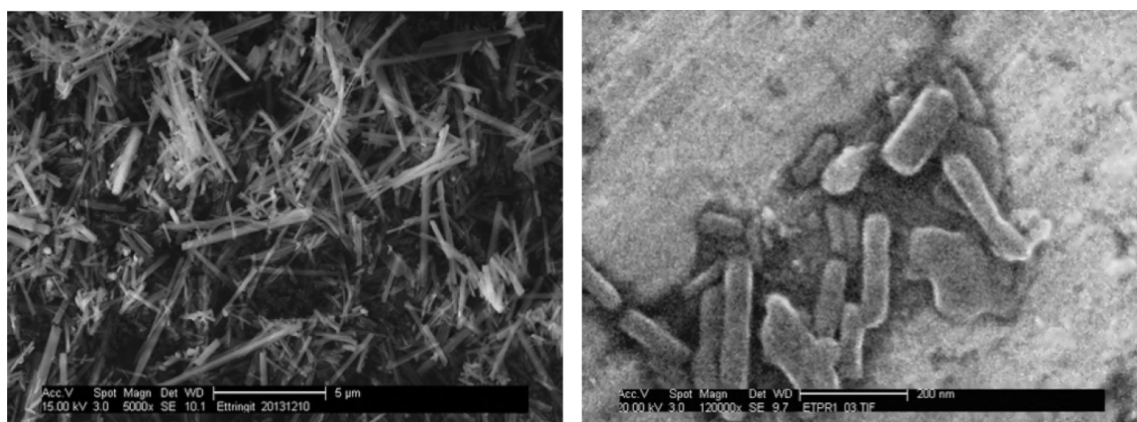
2.4.2 Ettringite from direct synthesis

Moreover Meier et al. (2016) and Bittnar et al. (2009) described the hydration of ettringite from C_3A and found that an addition of PCEs leads to a higher amount of nano-sized ettringite crystals after 10 seconds of hydration. They showed that PCE addition leads to a growth inhibition effect and smaller crystals with a length of less than 200nm and

an aspect ratio of 3.5. Meier et al. (2016) concluded that PCEs with a higher affinity increase the inhibition effect. Without PCE, ettringite precipitated with a crystal length of $3.8\mu m$. It was suggested, that some PCEs adsorb preferentially on the top and bottom of the crystals, leading to a smaller aspect ratio. The nano-sized ettringite crystals with a much higher surface area lead to the demand of more PCEs for the same dispersing effect. This could be the reason of the incompatibility of PCEs for some concretes (e.g. concrete with high C_3A content or HPC).

2.5 Influence of PCE during cement hydration

Zingg et al. (2009), Winnefeld et al. (2007) and Regnaud et al. (2011) showed, that the retardation effect from SP in cement is influenced by the content of C_3A and alkalis in the mix. The reason for that is that SP show an affinity for aluminate phases such as ettringite. By the adsorption of the SP on the anhydrous silicate clinker phases (C_3S and C_2S) the hydration mechanisms to create C-S-H and CH get blocked which retards the cement hydration Gelardi et al. (2015). How the interaction of aluminates and PCEs are influencing cement retardation, was quantified by Marchon (2016) and can be seen in figure 2.6.



(a) Shows the SEM image of ettringite from C_3A hydration from Brittain et al. (1968). Big crystals with an aspect ratio of 20 are shown.

(b) Shows the ettringite from Brittain et al. (1968) coming with the same solution as the left picture only with PCE addition. The crystal is around $200\mu m$ long with an aspect ratio of 3 – 5

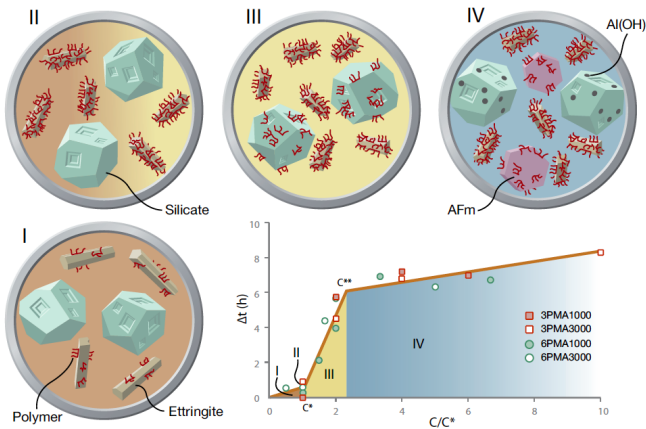


Figure 2.6: Influence of ettringite on silicate hydration with respect to adsorption affinity from Marchon (2016). stage I: almost no retardation of the hydration process as almost all PCEs adsorb only on ettringite until all ettringite surface is occupied by all the PCE dosed (c^* or II). Stage III: PCEs start to adsorb on silicate surfaces as well until critical saturation c^{**} is reached. During this process retardation occurs. Stage IV: A plateau is reached that correspond to the retardation due to an undersulphated system. AFm phases appear that attract PCEs.

The behavior of PCEs in the changing environment of cement hydration is influenced by the competitive adsorption with other chemical admixtures or ions (e.g. hydroxil ions and sulphate ions).

3 Material and Methods

3.1 Synthesis of ettringite

Two different kinds of ettringite samples were prepared in this study. One the one hand a sample from reaction of C_3A with hemihydrate. On the other hand a simplified system was created by using a direct synthesis of ettringite. Thereby no dissolution of anhydrous phases had to be taken into account. Aluminum sulphate octadecahydrate and calcium oxide were used for this second synthesis. All samples from the direct synthesis show the same water to solid w/s ratio, except one sample with 15% (w/w) 3PMA1000 addition and a w/s ratio of 15.

In the direct synthesis calcium oxide (CaO) was dissolved in water with a w/s ratio of 867.73 for one hour. Calcium chloride ($CaCO_3$) was burnt at 900°C for 7h to receive CaO. Afterwards aluminium sulphate octadecahydrate ($Al_2(SO_4)_3 \cdot 18H_2O$) and sometimes PCE were added with a w/s ratio of 31. The water to solid (w/s) ratio of the total solution was 312. A set-up is shown in figure 3.1a. For the other samples, ettringite was precipitated using C_3A and hemihydrate by using the more (500) or less (50) w/s ratio.

For every other solution with superplasticizer, the PCEs 3PMA1000 and 3PMA3000, which specification can be seen in table 3.1, were added in different dosages. The side chains (SC) of those two PCEs consist of Polyethylenglycol (PEG) and are connected to a single backbone. The hydrophilic character of the PEG, lets the side chains disperse in the solution. This research uses polymethacrylic acid (PMA) as the functional group. In comparison to acrylic based copolymers, methacrylic acid results in PCE that is more stable towards hydrolysis of the side chains. This way it is hoped to maintain the structure of the polymer throughout the hydration in the high pH solution. The PCEs were synthesised by esterification of the PEG on to the backbones that were polymerized previously.

A summary of all the samples synthesized in this work can be seen in appendix A. Special care was taken to reduce carbonation of the synthesized ettringite during sample preparation and storage, but could not be completely avoided. The process of ettringite synthesis can be divided into mixing, filtering and drying.

3.1.1 Mixing

Ettringite has been mixed in two different ways. Either a magnetic stirrer or an overhead stirrer were used. pH measurements with Gelardi et al. (2015) have been carried out to assure a pH of 11 which is required for ettringite formation. Bittnar et al. (2009) found that a delayed PCE addition of 1 minute lets ettringite grow to its normal size which is why a delayed addition wasn't considered in this report. At first a similar approach as in Mantellato et al. (2016) was taken, where a stirring time of 4h was used for the ettringite

synthesis.

Table 3.1: Specification of superplasticizer. Abbreviations can be seen in figure 2.4b

	C/E	P	MPEG Mw g/mol	N	n
3PMA1000	3.2	23	1000	4.2	14.8
3PMA3000	3.4	68	3000	4.4	13.9

3.1.1.1 Magnetic stirrer

A magnetic stirrer was used to mix the samples of 250 or 500g for different times. An example of the stirring bottle is shown in figure 3.1a. A magnet is put into the bottle with solution. The bottle is sealed and then put on to a generator that turned the magnet through a magnetic field.

3.1.1.2 Overhead stirrer

Some samples were prepared in a flask using an overhead stirrer to ensure good stirring and less carbonation. Those samples are labelled with an F in appendix A. The equipment used can be seen in table 3.2. The stirring shaft with the half moon blade was put through the middle neck of the round bottom flask and sealed using a joint sleeve and a stirrer bearing. Another neck was connected to the valve–flask adapter, which was kept closed in the beginning. Afterwards an ordinary balloon was filled with nitrogen and attached to a cannula. Then the reactants were put into the flask. After opening the valve–flask adapter, a rubber sleeve was used to close the last neck and the cannula with the balloon was stuck into it. The overhead stirrer was started using 200 turns per minute. As the nitrogen circulated through the flask the balloon had to be replaced with a new one every two hours. Three nitrogen balloons were used until the flask was closed.



PCE
 $Al_2(SO_4)_3 \cdot 18H_2O$
CaO



(a) Set up of the sample used for magnetic stirring and the relative amount of $Al_2(SO_4)_3 \cdot 18H_2O$, CaO , PCE and water.

(b) Vacuum-filtration of ettringite through filtration paper with 0.45 μm pore size. Pores are arranged in a flower-like form.

Table 3.2: Parts of the overhead stirrer

Item	Product ID	specification
PTFE Stirrer Blade	Wilmad L. LG-9510T-104	Half-moon, for 10 mm shafts
Polished Glass Stirrer Shaft	Wilmad L. LG-9501-100	44,5cm length, 10mm d.
PTFE Stirrer Bearing	Wilmad L. LG-9444-100	24/40 joint, 10mm diameter
3-neck Round-bottom flask	Wilmad L. LG-7331-194	24/40 joints, 1000ml
Valve - Flask Adapter	Wilmad L.s LG-1710-T202	24/40 joint
Flex-Shaft Stirrer Adapter	Kimble 7880200021	8-10mm
Rubber Sleeve	Kimble 774261	24/40
Lab Jacks	Fisherbrand S63080	10x10cm
Cork Support	Fisherbrand 07-835A	11 cm O.D.
PTFE Joint Sleeve	Scientific Machine 333-08	24/40
Overhead stirrer	IKA 0004442000	IKA EUROSTAR 20

3.1.2 Filtering

Vacuum filtration with a filter paper of 0,45 μm pore size was used. After mixing the solution was poured into the filter-cone seen in figure 3.1b. During the filtration process it is assumed that non adsorbed PCE is removed. This has already been stated in Zingg et al. (2009) and Dalas et al. (2015) and especially occurs for PCE with a weak charge density. Zingg et al. (2009) reported that the PCEs in the solution, however, have a strong impact on the physical properties of the pore solution such as water cluster structure, viscosity and surface tension

3.1.3 Drying

Oven drying, vacuum drying or freeze-drying techniques are often used to efficiently remove water from samples and reduce carbonation. Due to too extreme conditions, however, also water from the ettringite structure, could be removed. Baquerizo et al. (2016) and Renaudin et al. (2007) investigated that the water in the ettringite structure is removed at around 60°C. Special care also needs to be applied when using solvent exchange to stop ettringite hydration (Zhang & Scherer (2011), Zhang et al. (2018)). The solvent needs to have a relatively small molecular size to avoid the risk of removing water from the ettringite structure (Scrivener et al. (2016)). In this report neither freeze drying nor solvent exchange was executed. Instead a saturated solution of calcium chloride CaCl_2 has been used to ensure a constant drying at room temperature and relative humidity of around 35%. The samples took three weeks until one month to dry. Using silica gel instead of CaCl_2 in a desiccator to accelerate the drying process was tested and lead to a much faster drying process. More information on the drying damage of cement paste can be read in Zhang & Glasser (2000).

3.2 Characterisation methods

The techniques that have been used to analyse the samples were:

1. Powder X-Ray Diffraction
2. Scanning Electron Microscope
3. BET gas adsorption
4. Thermogravimetric analysis
5. Raman spectroscopy.

3.2.1 Powder X-Ray Diffraction

Powder X-Ray Diffraction is one of the most used and reliable techniques for quantitative phase analysis (QPA) on fine powder such as cement ([Scrivener et al. \(2016\)](#)). In this method a X-ray incident beam is shot on a crystalline sample at different angles. The reflected (or diffracted) spherical waves are then measured by a detector. Figure shows how the incoming X-ray beam with an incident angle θ , coming from left, is reflected by the individual atoms of the sample. The distance between different atom layers is material specific and called d-spacing.

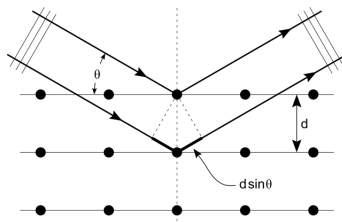


Figure 3.1

For certain angles more waves are reflected than for others (overlapping of waves reflected from atom layers with certain d-spacing). The result is a XRD pattern with number of counts per 2θ and is used for further analysis. The crystalline phases of a material can be identified by comparing the resulting peaks at specific incident angles with known data of a material in the literature. The peak intensities are influenced by the nature and disposition of molecules. A more amorphous material can be presumed if the background noises of the XRD pattern are higher and the peaks are less distinct. To quantify the amount of crystal phases an external or internal standard method has to be used. Using Bragg's law in equation 3.1 the incident angle 2θ and the measured wavenumber can be used to calculate d-spacing of the sample.

$$2d \cdot \sin(\theta) = n \cdot \lambda \quad (3.1)$$

Where n is a positive integer and λ is the wavelength.

For XRD measurements the dry ettringite sample has to be grind finely and placed in the sample holder by not changing the crystal orientation on the surface. A $CoK\alpha$ radiation ($\lambda = 1.79$) was used at $40kV$ tension and a current of $40mA$. Furthermore a $240mm$ goniometer radius, a 2θ step size of 0.001 , a 0.04° fixed divergence slit angle and a X'Celerator detector was used. Data was collected in a 2θ data range of 3° to 80° .

Analysing XRD patterns

The XRD pattern of the sample was analysed using the software X'Pert Highscore Plus. To compare the peaks, the references in table 3.3 were used.

Table 3.3: Data from the American Mineralogist Crystal Structure Database in [Micaela \(2015\)](#) was used. The X-ray diffraction peaks can also be found in [AMS \(1992\)](#)

Material	Literature
Ettringite	Moore & Taylor (1970) , Hartman & Berliner (2006)
Gypsum	Schofield et al. (1996) , Boeyens & Ichharam (2002)
Calcite	Sitepu et al. (2005) , Graf (1961)

The software was used to determine the background and fit the peaks of the XRD data. Afterwards Rietveld refinement was used to identify the amount of crystalline phases in the sample. A theoretical line profile is calculated by the software using the least squares method. This curve is than fitted to match the XRD data by changing different structural parameters like crystal orientation (a,b ad c) and size. For the analysis of the ettringite samples in this work, the following parameters were refined in a semi-automatic method: scale factor, zero shift, lattice parameters, background, profile parameters W,U and V (Halfwidth), peak shape parameters and the preferred orientation. The background was determined with a granularity of 4 and a bending factor of 1. A Pseudo Voigt profile function and a profile base width of 10 was used. Thereby a weighted R profile between 10 and 12 was obtained for most samples. The measurement accuracy of XRD and Rietveld refinement is around 1%.

3.2.2 Scanning Electron Microscope (SEM)

Scanning electron microscope is used in this research to analyse the changes in morphology of ettringite needles through the influence of PCE ([Scrivener et al. \(2016\)](#)). The SEM uses an electron beam that is shot on a sample under high vacuum. Depending on the depth that the electrons enter the sample, different signals can be measured. Those are secondary electrons (SE), back scattered electrons (BSE) as well as characteristic X-rays. In this work only the SE images were observed. Thereby an incident electron knocks an electron out of its shell which is then collected by a detector. The sample thereby has to be conductive, which is why ettringite was coated with a carbon layer. Only the SE from the surface ($<50nm$) can be detected. The amount of electrons that leave the sample depends on the surface of a specific spot. For instance, because edges have more surface then smooth planes, they are likely to release more electrons. The more electrons are reaching the

charged detector, the brighter the sample will appear. An image is created as the electron beam scans over the surface of the sample and shows the topography of the sample.

For the samples very little amount of dry powder was placed on a sample holder which subsequently was put into a carbon coater for around 20 min. Thereby a 15-20 nm thick carbon layer was added. The SEM machine used was a Zeiss EVO Variable Vacuum Instrument -10 with a tungsten filament. A voltage of 5kV was applied. The best working distance was at around 10.5mm.

3.2.3 BET gas adsorption

BET specific surface area (SSA) measurements were made to investigate the surface area per gram of synthesized ettringite. Nitrogen was used as an adsorbate gas and circulated through the sample until nitrogen atoms have adsorbed on the sample. The energy to release the nitrogen atoms in the sample rises when more layers of adsorbed nitrogen molecules are added. Depending on how much nitrogen was released into the sample the amount of surface area can be calculated.

The measurements were performed using a BET multi-point (6 points isotherm) nitrogen physisorption device (Micromeritics Tristar II 3020). The sample had to dry and were degassed with an external degassing station (VacPrep 061, Mircomeritics) at 40°C with N_2 flow for 16h. BET measurements thereby have an error of $\pm 2\%$ [Material \(2012\)](#).

3.2.4 Thermogravimetric analysis

Thermogravimetric analysis (TGA) is a common measurement technique in cement science ([Scrivener et al. \(2016\)](#)). Thermal reactions of a sample like dehydration, dehydroxylation, decarbonation, oxidation, decomposition, phase transition or melting can be measured. While the sample and an inert reference is heated up, the weight loss is recorded, which can be related to the loss of H_2O , CO_2 as well as redox- or recrystallization reactions. In cement science TGA is used to identify hydration phases and the presence of crystalline and amorphous phases. It is used in this report to confirm XRD measurements. The differential thermogravimetry (DTG) which is the derivation of the thermogravimetric (TG) data allows a better identification of the results.

Ettringite loses water between columns at around 100°C (table 3.4). The water lost from the dehydroxylation of aluminium hydroxide occurs between 200°C to 400°C with a main weight loss at around 260°C. Decarbonation occurs at higher degrees between 600°C to 800°C, but in ettringite usually only goes up to 750°C ([Scrivener et al. \(2016\)](#)). According to [Goto et al. \(1995\)](#), aragonite and vaterite (both less common crystalline polymorphs of calcium carbonate) recrystallize without weight change at 450°C to calcite. The loss of water in ettringite during TGA is significant. Starting from a molecular weight (MW) of 1255 $\frac{g}{mol}$ it loses around 576 $\frac{g}{mol}$ or 45.9wt% of water. Gypsum ($CaSO_4 \cdot 2H_2O$) loses water between 100°C and 140°C as well as between 140°C and 150°C. It thereby overlaps with the water loss of ettringite. During the first step it turns to hemihydrate ($CaSO_4 \cdot 0.5H_2O$) and during the second step to anhydrite ($CaSO_4$) (usually both processes overlap strongly).

Table 3.4: Temperature range of main weight loss of ettringite

H_2O between columns	100°C
H_2O dehydroxylation of aluminium hydroxide	200 – 400°C
CO_2	600 – 750°C

3.2.5 Raman spectroscopy

Raman spectroscopy is a vibrational spectroscopy and is used to examine material specific molecular bondings in a structure. The following information can be obtained:

- the presence of known compounds (fingerprint).
- structure of ettringite
- properties of bonds (bond strength, force constants)

During Raman measurements monochromatic light is shot on a group of atoms. From the photons that hit the atoms some energy is used to change their molecular vibration and the rest is scattered as inelastic or elastic light. While the elastic scattered light (called Rayleigh scattering, accounting for 99% of the scattered light) has the same energy as that of the incoming light, the inelastic scattered light (called Raman scattering, around 1% of the scattered light) has a different energy than the incoming light. The elastic scattered light does not modify the final energy state or frequency of the spectral line of an atom. This is because the excited electron of an atom returns to its original vibrational level and the thereby emitted photon has the same energy as the incoming photon. The elastic scattered light is filtered out in Raman measurements. Never the less, the inelastic scattered photons show a shift in energy between the incoming and the outgoing photons. This shift is called Raman shift and changes the vibrational level of an electron. The Raman shift is represented in wavenumbers (cm^{-1}), which is the amount of waves per one centimetre. Two energy shifts are possible. The incoming photons can either gain energy (higher frequency) or lose energy compared to the incoming photon. In the first case, a so called "Anti-Stokes" shift appears as the energy state of the atoms decreases. In the second case the vibrational levels of the atoms are raised. Thereby a lower frequency in the spectral line of the atoms occurs, which is called Stokes shift. The Stokes shifts are relatively strong and positive and generate a molecular fingerprint of a sample. Atoms can have different vibrational modes that depend on the chemical bonds with other atoms. The frequencies of the vibration depend on the masses of the atoms and the strength of the bonds (light atoms with strong bonds show high Raman shifts). A reference database is required to identify the peaks of the Raman shift. The papers that were used to identify the peaks of ettringite can be seen in table 3.5.

Table 3.5: Literature for helping identifying ettringite and PCE peaks

Phase	Literature
Ettringite	Black et al. (2006), Renaudin et al. (2007)
Calcite	De La Pierre et al. (2014), Behrens et al. (1995)
PEG	Koenig & Angood (1970)
PMA	Corporation et al. (1969), Taylor (1973)

The *P31c* trigonal description of ettringite indicates that in each unit cell, three sulphate anions are crystallographically independent. Renaudin et al. (2007) investigated ettringite with Raman spectroscopy and showed that the main sulphate peak ($v_1(SO_4^{2-}$ at 989 cm^{-1}), indeed was best fitted with three curves. This, indicating three independent sulphate bonds, the trigonal space group could be confirmed.

The machine used for Raman spectroscopy was a Horiba Jobin Yvon LabRam. The excitation line was provided by a HeNe laser at 632.8 nm, through a 100x objective with 0.8 numerical aperture. The detector was calibrated with the 520.7 line of a silicon standard.

4 Results

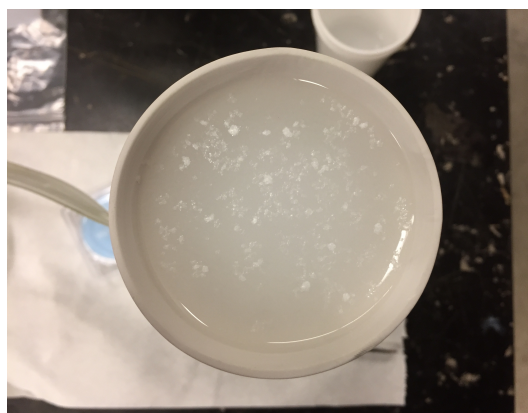
This chapter shows the results of the synthesized ettringite samples seen in appendix A. The ettringite samples are thereby referred to as "A_{Ft}" if no PCE and "A_{Ft}+PCE" if PCEs are added into the solution.

4.1 Filtering

Figures 4.1a and 4.1b show the solution of ettringite with and without PCEs after four days of synthesizing. In figure 4.1a, ettringite crystals agglomerate on the surface of the water. In this system no PCEs are present. The solution with PCEs can be seen in figure 4.1b. There, no sample showed agglomeration of particles. This is because of the strong dispersing effect from the PCEs. This findings correlate with Bittnar et al. (2009). The filtration time for A_{Ft}+PCE solutions was higher and increased strongly over the stirring time (30x higher after 5 days), the filtration time of A_{Ft} stayed relatively constant and short.

4.2 X-Ray Diffraction

XRD was used to analyse the chemical composition of the samples and assure that stable ettringite was formed. Figure 4.2a shows the results of ettringite from 500ml solutions with and without 2% of 3PMA1000. Besides ettringite, gypsum and calcite could be observed in the samples. As can be seen in figure 4.2a, a 4h hour stirring time, did not lead to a



(a) Filtering of ettringite solution without PCE

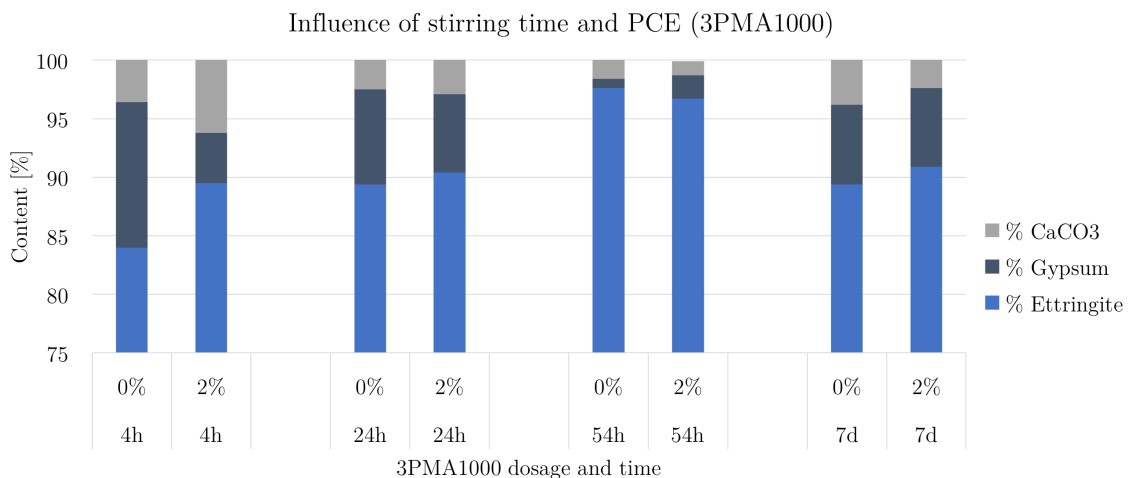


(b) Filtering of ettringite solution with PCEs

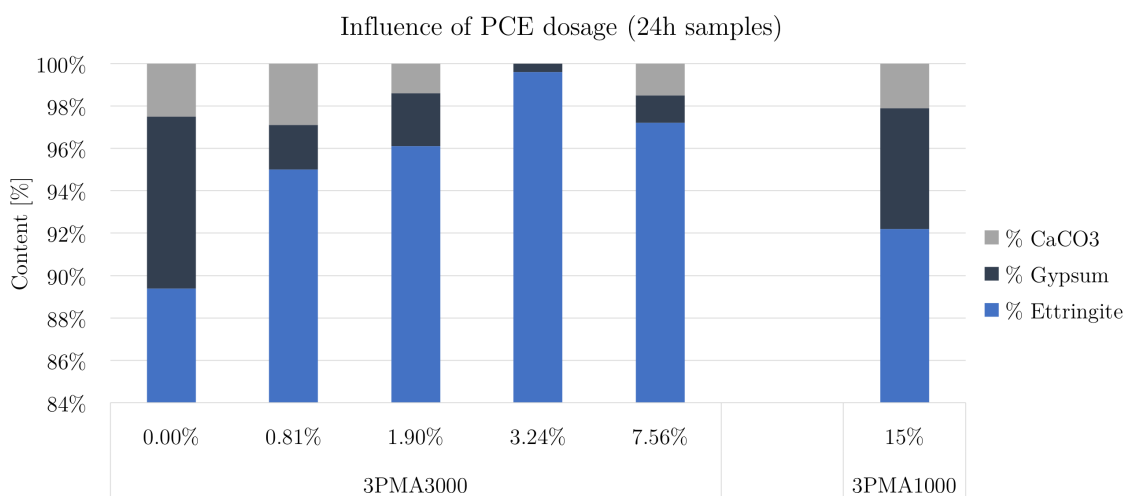
Figure 4.1: Ettringite solution during filtering without (left) and with (right) PCE.

sufficiently high enough purity. While better results were obtained for 24h and 54h stirred samples a synthesis of 7 days decreased the relative amount of crystalline ettringite, which might be related to the transformation from AFt to AFm. Due to the long drying time it was not possible to further optimize the quality of the ettringite samples. A 24h stirring time was chosen for further samples and lead to better results for smaller solution volumes (250ml instead of 500ml).

Figure 4.2b shows the effect of the PCE 3PMA3000 dosage on the relative amount of AFt precipitated after 24 hours of stirring. More stable ettringite was reached. The better results might also come from the smaller solution size of 250ml (at same w/s ratio) used for those samples. A decrease of stable AFt can be seen at high PCE dosage. For the addition of 15% SP, the 3PMA1000 was used, which is why it is separately shown in the graph. For this sample 92.2% stable ettringite with 2.1% calcite was observed.



(a) The percentage in weight of crystalline ettringite in samples with and without PCE and different stirring time, measured by XRD.



(b) Percentage in weight of ettringite in samples that were stirred for 24 hours, with different dosages of 3PMA3000.

Figure 4.2: XRD results for ettringite from direct synthesis

XRD from results of ettringite precipitated from C_3A

The yield of ettringite synthesised by C_3A can be seen in figure 4.3. The two samples on the left had a higher w/s ratio (500 vs. 312 from direct synthesis) and show less stable ettringite. The other three samples show better results and had a lower w/s ratio (50 vs. 312 from direct synthesis). All samples were stirred for 5 days and no clear influence from the PCE can be seen in the XRD results.

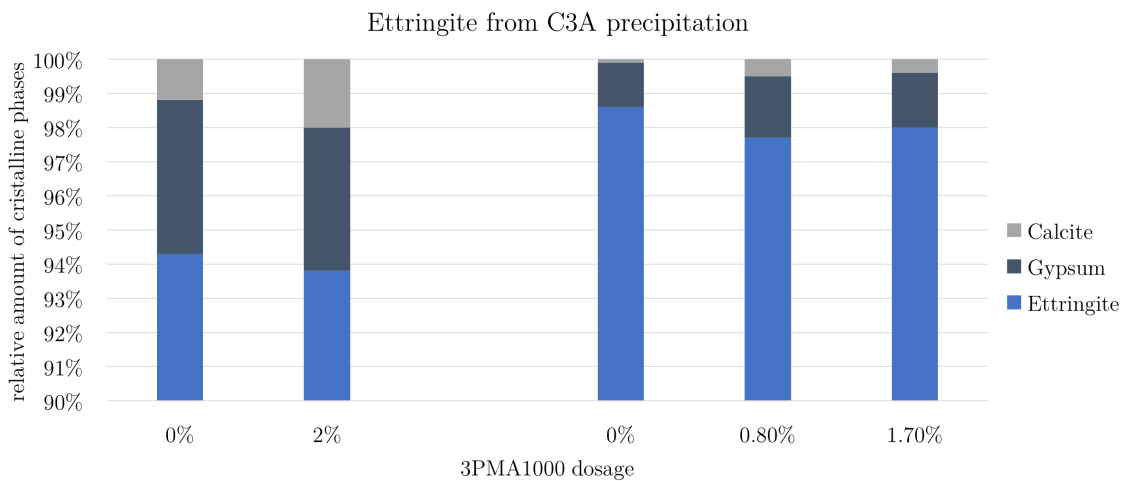


Figure 4.3: XRD results from ettringite precipitated from C_3A and hemihydrate. All samples were stirred for 5 days. Different amount of 3PMA1000 was added to the samples. The two samples on the left had the same w/s ratio as the directly precipitated ettringite, while the three samples on the right had a lower w/s ratio.

4.3 TGA

An example of the TGA results can be seen in figure 4.4 from the sample with 3.24% (w/w) 3PMA3000. This sample was chosen, because it showed good XRD results with 99.6% stable AFt and a weighted R value of 10.31. Two peaks are associated to the water release of the ettringite structure (marked in red), which contributes to around 45% of its weight. The first sharp peak at around $100^\circ C$ is related to the water loss in the inter-columnar region and the peak at $260^\circ C$ is associated to the intra-columnar region. All samples show carbonation between 600 and $775^\circ C$ (marked in grey). In some cases the peak at $100^\circ C$ is deformed or a second peak can be seen at around $130^\circ C$ (marked in blue). This peak was associated with the water loss from gypsum in the system. The CO_2 release was used to quantify the amount of calcite in the system, which was then compared to the XRD results. Therefore the stoichiometric equation 4.1 was used.

Furthermore TGA measurements on pure 3PMA1000 have been carried out. The results show a peak which was associated to the decomposition of the PCE between 400 and $450^\circ C$. This peak, however, could not be seen at the TGA results of the AFT+PCE sample with 15% (w/w) of 3PMA1000.

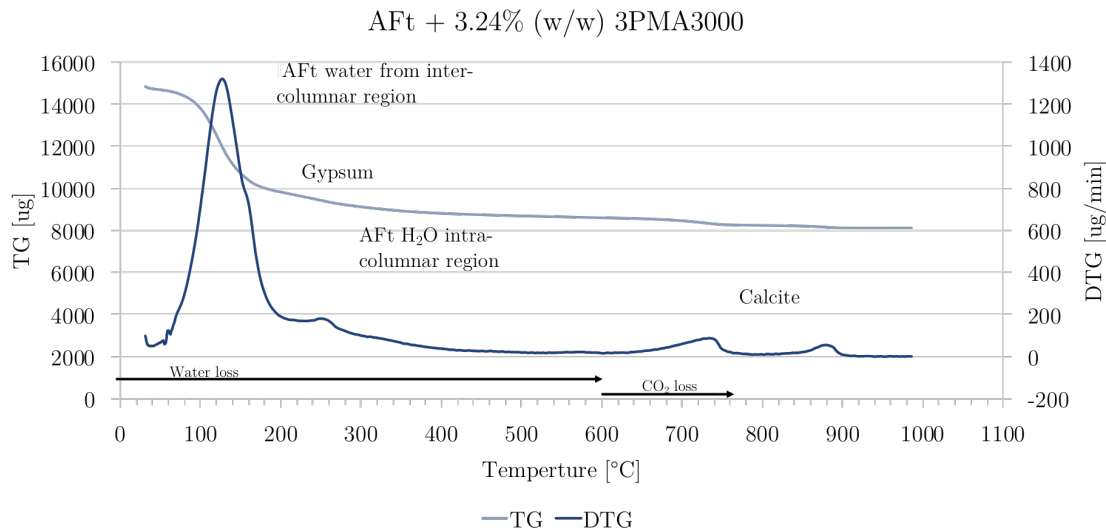


Figure 4.4: TGA results of ettringite with 3.24% (w/w) 3PMA3000. The water loss of the inter and intra-columnar region of AFt as well as the calcite peak between 600 and 775 °C can be seen. Another influence comes from the gypsum in the system at around 130 °C

4.4 Morphology analysis

As a result of the fine powder, especially for the samples with PCE addition, high charging occurred during the SEM measurements. This section is divided into several subsections. At first it was divided in ettringite samples from direct synthesis and from C_3A and hemihydrate reaction.

4.4.1 Ettringite from direct synthesis

4.4.1.1 3PMA1000

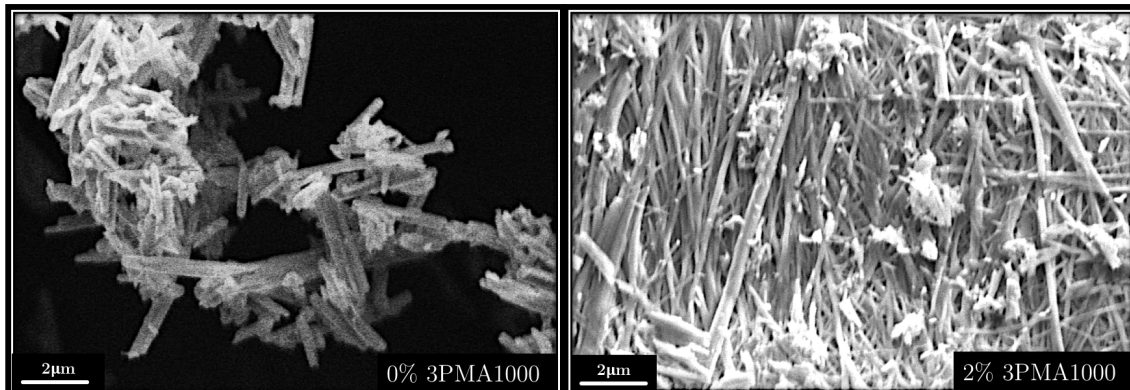
2% (w/w) 3PMA1000 addition using the magnetic stirrer

The first two figures 4.5a and 4.5b show the influence of 2% 3PMA1000 on directly synthesised ettringite using a magnetic stirrer. After 24 hours ettringite crystals usually have a length of around 2 μm and width of 0.25 μm , which is also the case in the left pictures of figure 4.5a

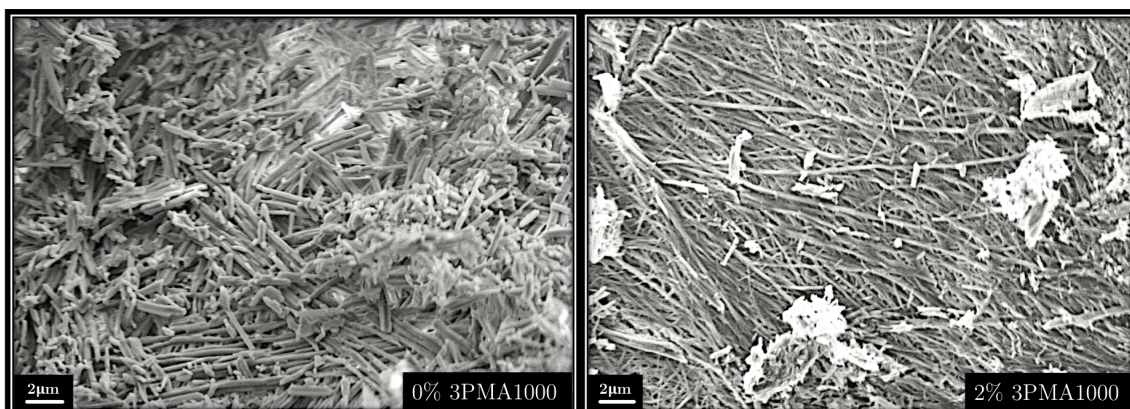
An addition of 2% 3PMA1000 clearly affects the morphology of the crystals. They become much thinner and longer. The right pictures of figure 4.5a and 4.5b show examples of such

fiber-like crystal needles. Up to 18 μm long and 0.15 μm wide ettringite needles could be observed by PCE addition.

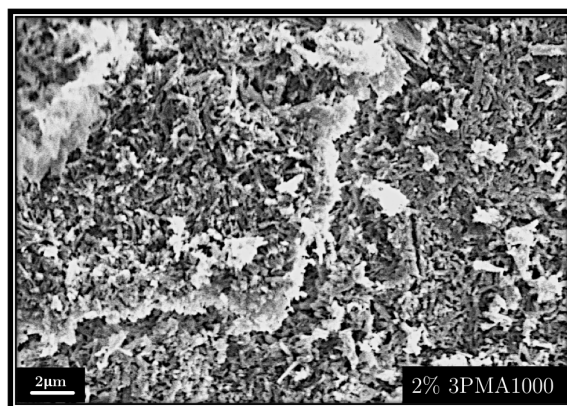
Figure 4.5c showed a different morphology of AFt crystals with 3PMA1000 addition. Here the crystals didn't grow in length. They are slightly smaller in width and stay shorter. All this samples used a w/s ratio of 500.



(a) Morphology of ettringite needles without and with addition of 2% (w/w) 3PMA1000. Long short fiber-like needles can be seen as an effect of PCE addition on the right



(b) Morphology of ettringite crystals without and with addition of 2% 3PMA1000 at a higher scale. Similar effect as in figure 4.5a



(c) A different effect of PCEs on the crystal structure of AFt. Crystals become shorter and thinner

Figure 4.5: Ettringite morphology without and with addition of 2% (w/w) 3PMA1000

2% (w/w) 3PMA1000 addition using the overhead stirrer

Preparing the ettringite from direct synthesis with 2% (w/w) 3PMA1000 in the flask, while using the overhead stirrer showed only fiber-like ettringite needles. Two examples are shown in figure 4.6.

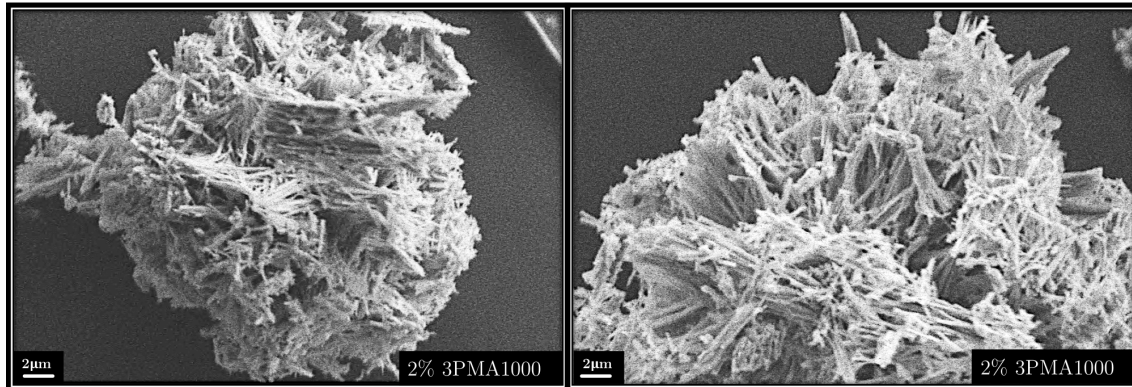


Figure 4.6: Ettringite crystals from direct synthesis prepared in the flask. Thin fiber like needles can be observed.

15% (w/w) 3PMA1000 using the magnetic stirrer

Figure 4.7 shows the SEM images of ettringite with a very high 3PMA1000 addition of 15%. The solution had a much smaller w/s ratio of 15. An agglomeration of very small particles can be observed and no needles can be seen.

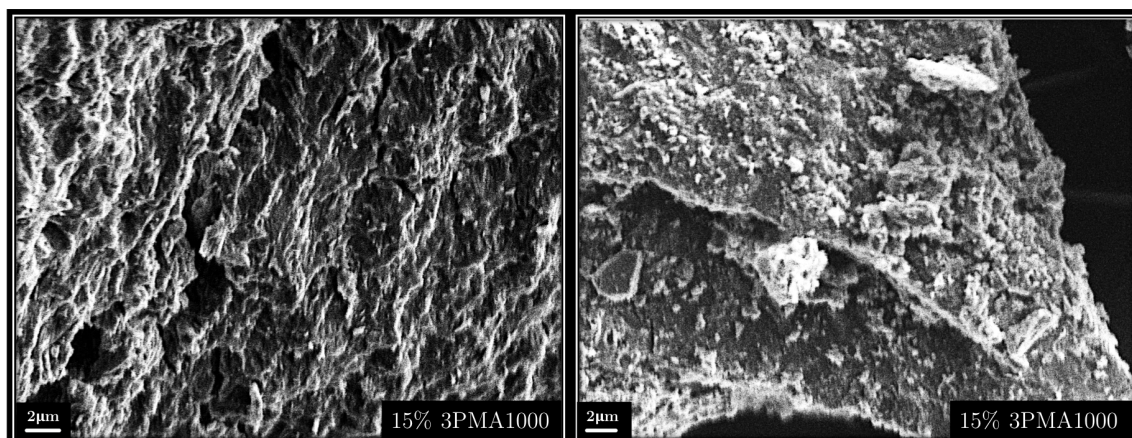
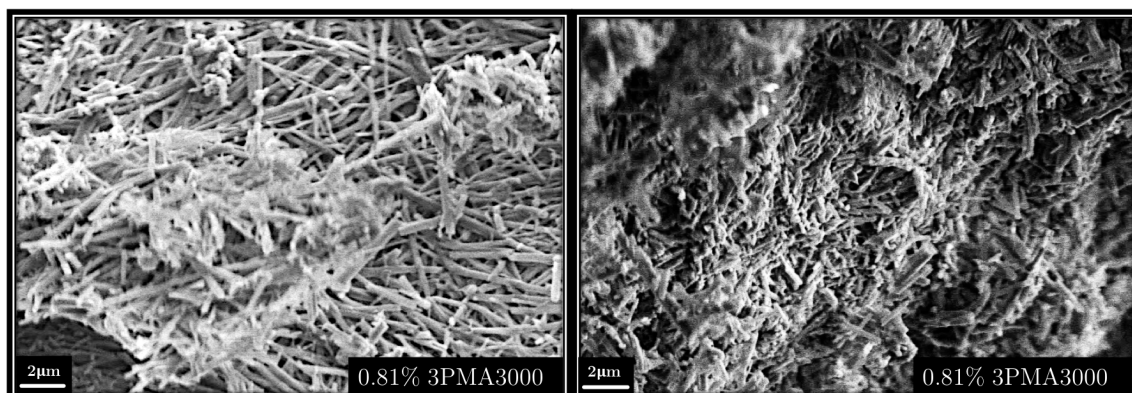


Figure 4.7: Ettringite with 15% addition of 3PMA1000.

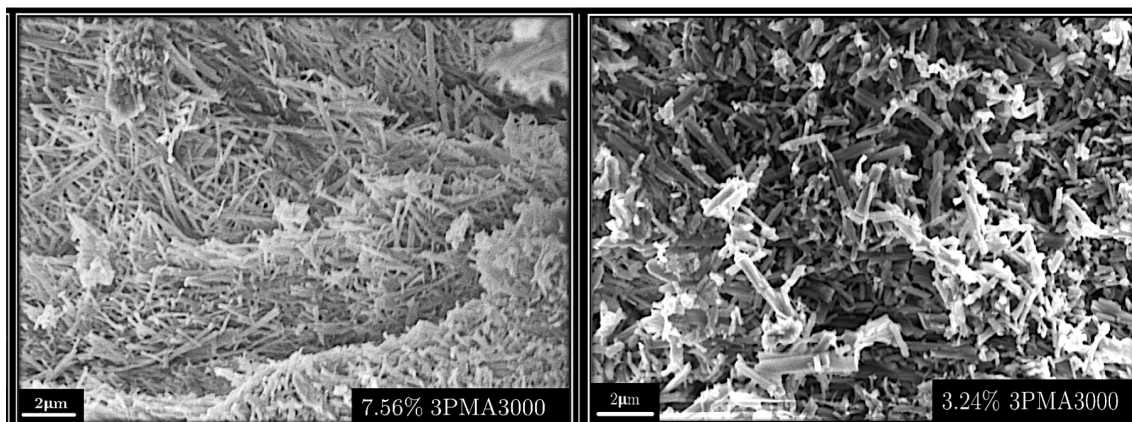
4.4.1.2 3PMA3000

Different 3PMA3000 dosages using the magnetic stirrer

Figure 4.8a shows two pictures of AFt crystals with a 0.81% (w/w) addition of 3PMA3000. The two different effects of PCEs on the morphology of crystals can be seen. While the left picture shows long needles, the right one shows and agglomeration of smaller particles. Figure 4.8b shows formation of crystals at higher 3PMA3000 dosage. On the one hand (left picture), ettringite needles get finer with higher dosage, on the other hand (right picture), also short AFt crystals that look like normal ettringite are formed. The short needles are not smaller than the one with lower 3PMA3000 dosage (picture above).



(a) Two different kinds of ettringite crystals for a 3PMA3000 addition.



(b) Comparing the ettringite structure with a different dosage of 3PMA3000. The crystal needles become thinner and more fiber-like. Also short ettringite crystals can be seen.

Figure 4.8: Ettringite morphology without and with addition of 2% (w/w) 3PMA3000

4.4.1.3 Influence of the molecular structure of PCEs

Figure 4.9 compares the effect of 2% (w/w) 3PMA3000 and 3PMA1000. A much stronger effect on the crystal morphology of ettringite can be seen for 3PMA1000. The crystal needles are much thinner and fiber like.

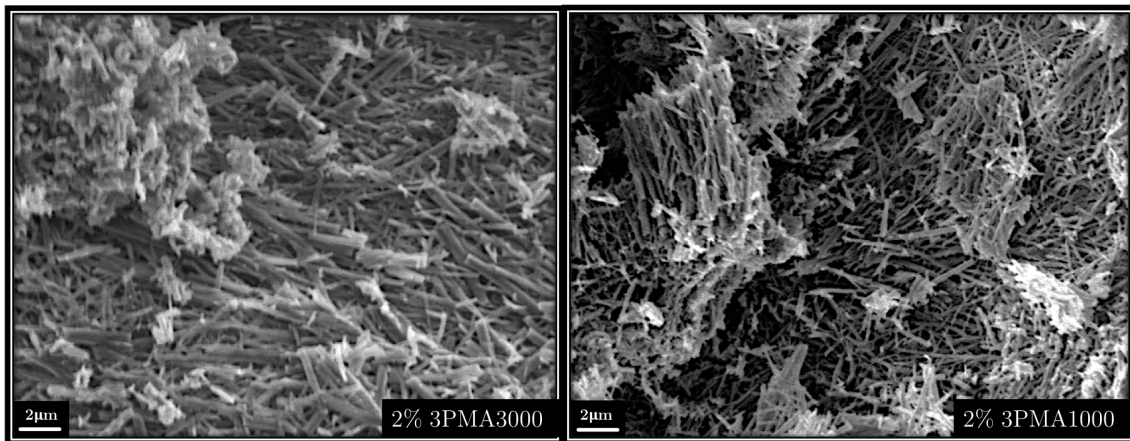


Figure 4.9: Effect of the molecular structure of PCE. In the left picture the effect of 2% (w/w) 3PMA3000 and on the right 2% (w/w) of 3PMA1000 can be seen.

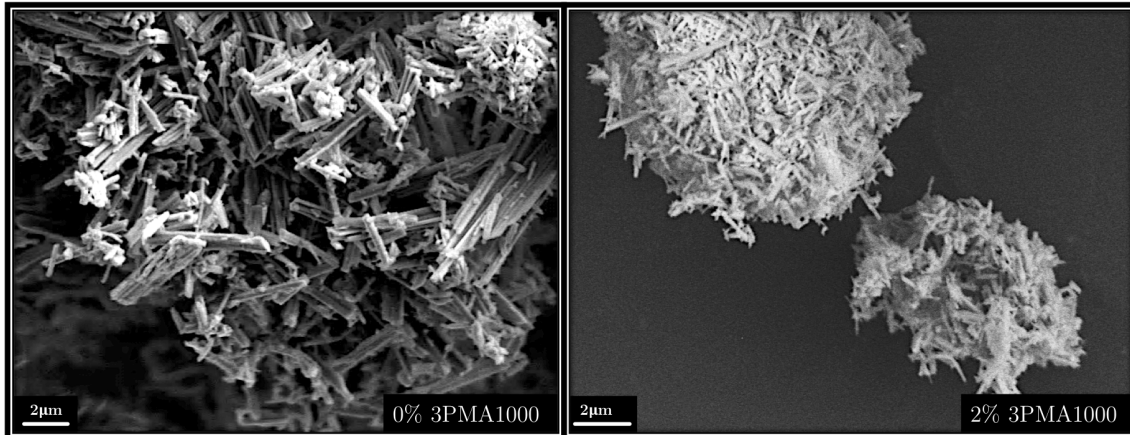
4.4.2 Ettringite from reaction of C_3A and hemihydrate

Ettringite was precipitated from the reaction between C_3A and hemihydrate using two different w/s ratios of 500 and 50, which were higher or lower than the directly synthesized sample w/s ratio of 312.

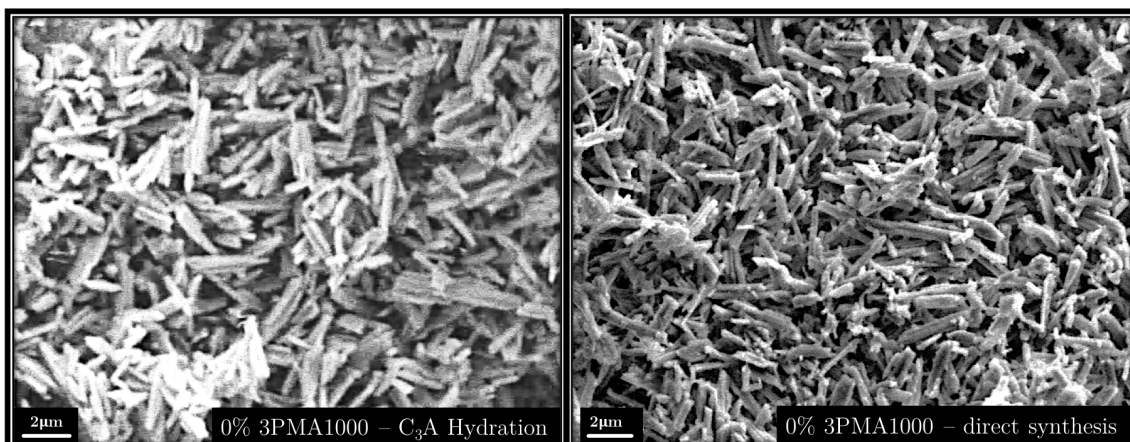
4.4.2.1 Solution with higher w/s ratio than the directly synthesized ettringite

The effect of the PCEs on the crystal structure of ettringite synthesised from C_3A (with higher w/s ratio as the direct synthesis) can be seen in figure 4.10a. The crystals become much thinner and seemingly more, when PCE is added (right picture).

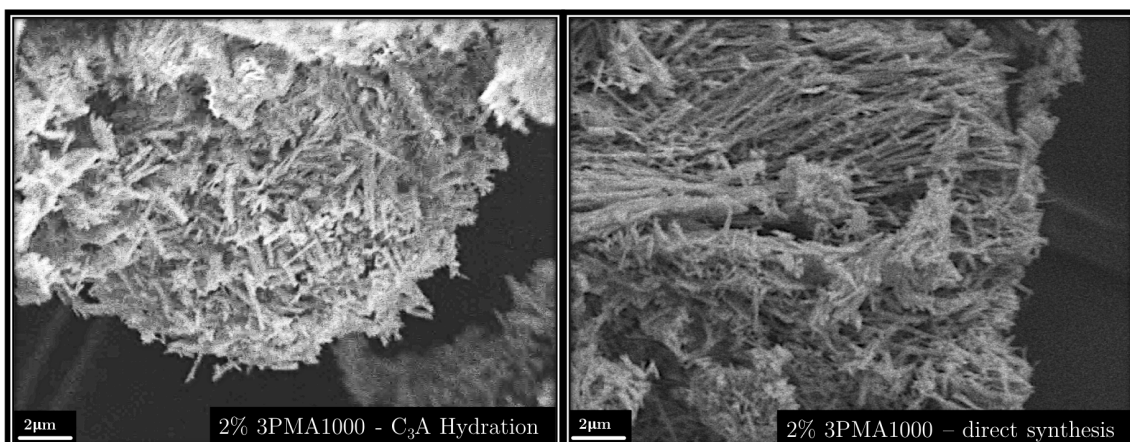
The influence of the w/s ratio difference between 500 and 312 is assumed not to make a big difference, which is why both synthesis methods were compared next. Figure 4.10b compares the samples without PCE addition. The crystals show a similar aspect ratio and size as the ones precipitated from direct synthesis. Figure 4.10c compares the results of the two precipitation methods with PCE addition. The left picture shows that the ettringite crystals from C_3A and hemihydrate reaction are shorter than the ones from the direct synthesis. No fiber-like crystal needles could be observed.



(a) The effect of 2% (w/w) of 3PMA1000 on the morphology of ettringite crystals precipitated from C_3A with a similar w/s ratio as the examples above.



(b) Comparison of ettringite needles morphology between direct synthesis and precipitation from C_3A without PCE.



(c) Comparing the ettringite crystals with 3PMA1000 addition of the two precipitation methods. While also having a fiber-like structure, the ettringite crystals coming from C_3A precipitation are shorter.

Figure 4.10: Ettringite from C_3A and hemihydrate reaction without and with addition of 2% (w/w) 3PMA1000 compared to the direct synthesis

4.4.2.2 Solution with lower w/s ratio than the directly synthesized ettringite

Figure 4.11 shows this effect of using a lower w/s ratio of 50, for increasing 3PMA1000 dosages. PCE addition again, leads to smaller and seemingly more crystals. Compared to the previous effects of PCEs, however, the crystals in this case are less thin and much shorter. Generally a smaller effect of the PCE can be observed.

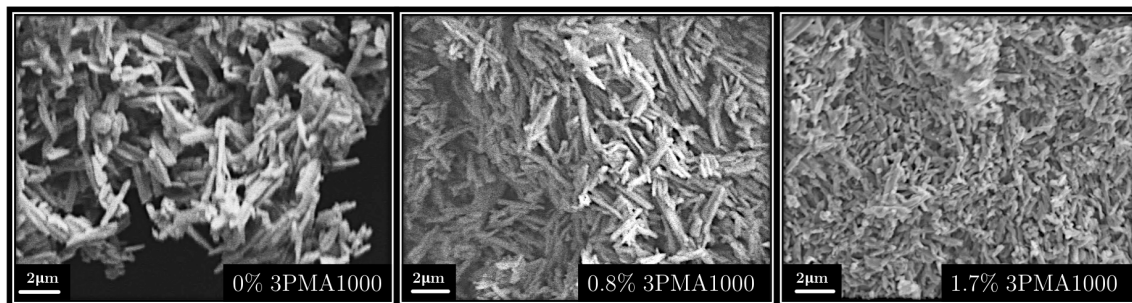
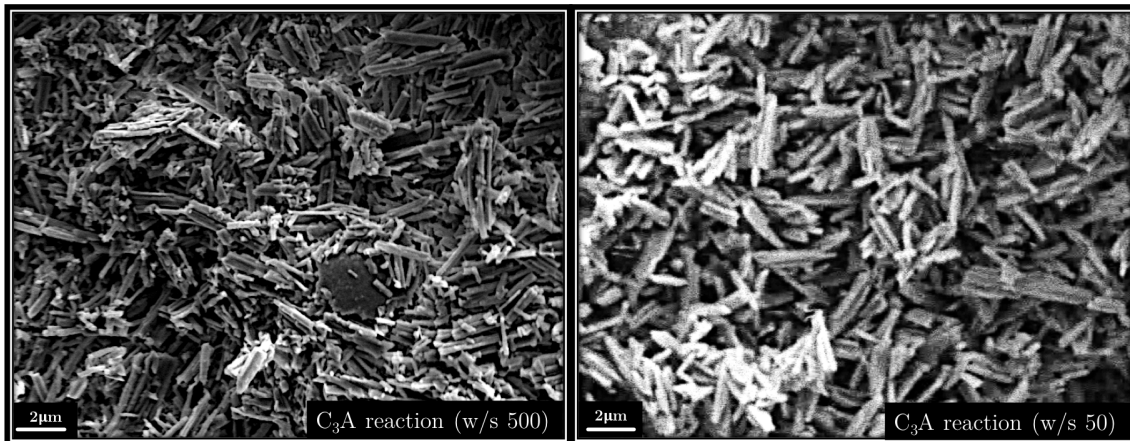


Figure 4.11: Ettringite crystals from C_3A reaction. A lower w/s than all other samples and from left to right an increasing amount of 3PMA1000. The samples were stirred for 5 days.

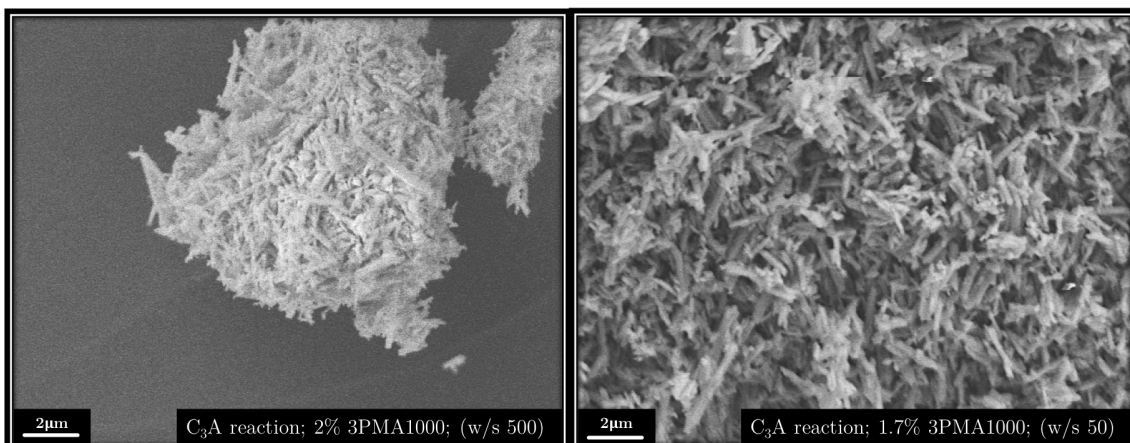
4.4.2.3 Comparing the different w/s ratios

Figure 4.12a shows the ettringite from C_3A reaction without PCE addition and with different w/s ratios. Look closely, slightly bigger crystals are revealed for the case with lower w/s ratio (right picture).

When comparing the ettringite from the two systems with PCE addition (figure 4.12b), once again, slightly bigger crystals could be observed for the samples with the lower w/s ratio.



(a) Comparison of ettringite needles morphology between ettringite of C_3A and hemihydrate reaction with different w/s ratio (left w/s 500 vs. right w/s 50).



(b) The effect of 1.7% and 2% 3PMA1000 addition to ettringite synthesised by C_3A reaction with different w/s ratios of 500 and 50.

Figure 4.12: Comparing ettringite from C_3A and hemihydrate reaction with different w/s ratios. Figure 4.12a without and figure 4.12b with 3PMA1000 addition.

4.5 BET gas adsorption

Figure 4.13 shows clearly that a PCE addition leads to a much higher SSA of ettringite with a ratio between 2.25 to 2.35. Furthermore, in the same graph, a decreasing SSA can be observed with increased stirring time for both AFT and AFT+PCE samples. Thereby the ratio in SSA between the samples remains the same.

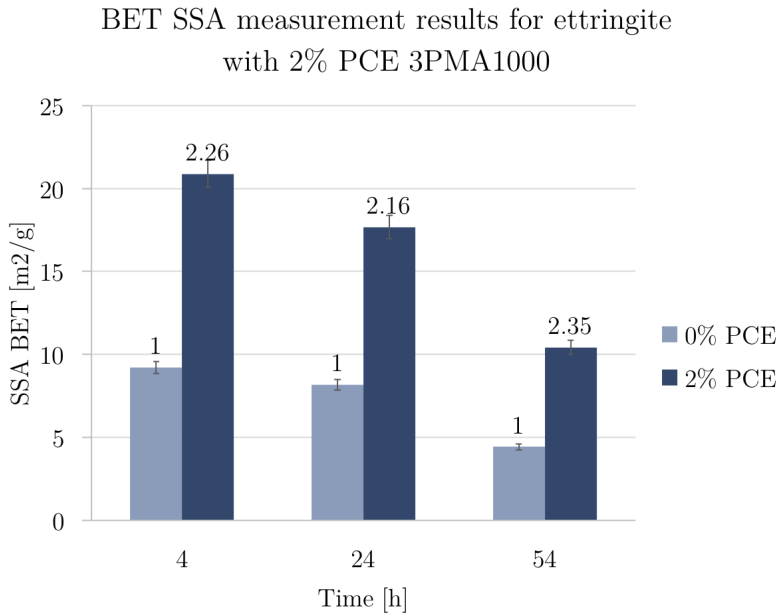


Figure 4.13: Results of the BET measurements of samples with and without PCE between 4 hours and 54 hours of stirring. A constant ratio between the samples at different stirring times can be seen

Figure 4.15a shows the influence of the dosage of two different PCEs on the specific surface area created. A linear increase can be seen with added PCE dosage. With increasing dosage, 3PMA1000 leads to a much steeper increase of SSA compared to the 3PMA3000. Figure 4.15b shows the results of BET measurements published by [Dallas et al. \(2015\)](#). There ettringite was synthesized from 16% C_3A , 4% $CaSO_4$ and 80% $CaCO_3$. The specification of the PCE C20s and the weaker PCE C38s can be seen in table 2.1. At the same SC length ($P=25$), C20s has twice as much C/E than C38s (5 vs. 2.6) and therefore a higher charge density (see table 3.1 to compare with the specifications of 3PMA1000 and 3PMA3000). The results of the different PCEs for 5min and 120min of reaction are similar to the results in this report. The SSA increases linear with PCE dosage. Furthermore the PCE with the higher charge density (C20s) show a steeper increase in SSA. Furthermore, the strong increase of the SSA after 5min of stirring is remarkable.

Figure 4.14 shows the SSA of the same samples as figure 4.15a and compares the SSA with the amount of carboxylates per gram of solid. Once again a stronger increase in SSA can be seen for ettringite with 3PMA1000 compared to 3PMA3000. This might be a problem that arises with higher dosage or a not linear relation of this polymer. To know which one it is, more measurements have to be taken.

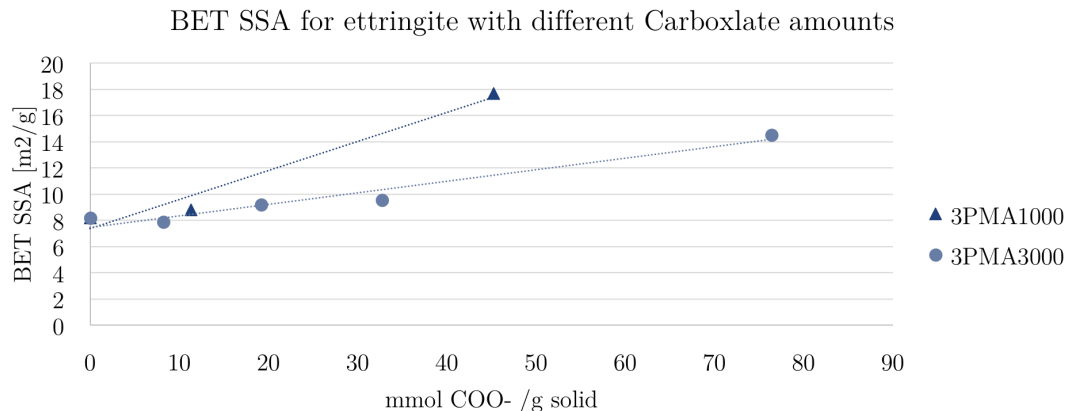
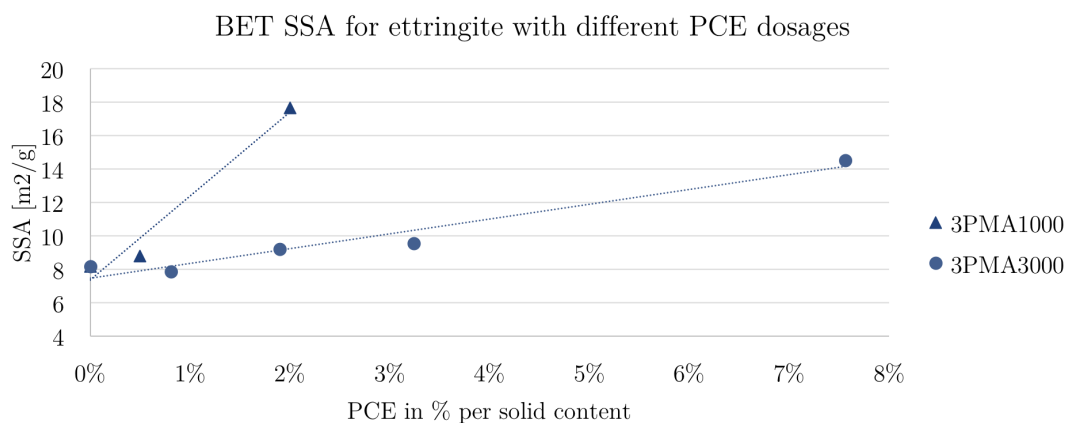


Figure 4.14: Comparing the SSA of ettringite by looking at the amount of Carboxylate groups per solid content.



(a) Comparing the SSA of ettringite using different dosages of 3PMA1000 and 3PMA3000 (% w/w) after 24 hours.

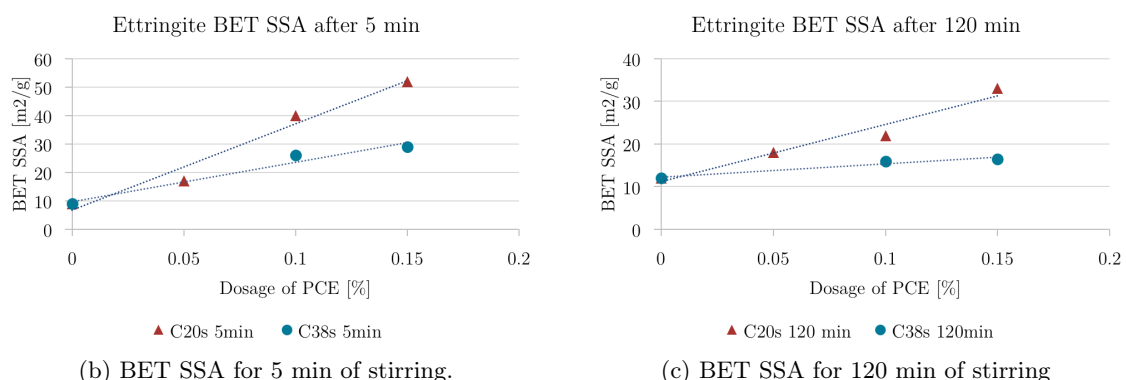


Figure 4.15: Comparing the effect of the dosage from different PCEs on the SSA after 24h (top). The results are compared to data received from [Dadas et al. \(2015\)](#) who investigated the SSA for the PCEs C20s C38s (see table 2.1) after 5min and 120 minutes of reaction.

4.6 Raman spectroscopy

Figure 4.16 shows the Raman shifts of ettringite from direct synthesis. The literature for the allocation of the peaks can be seen in table 3.5. Like in XRD and TGA, calcite (in grey) could be observed in the samples. The red and blue peaks are associated to ettringite. Four different vibrational modes of sulphate (SO_4^{2-}) in the inter-columnar region can be observed at 450, 605, 989 and 1114 cm^{-1} . Furthermore an aluminium ($Al - (OH)$) stretch at 550 cm^{-1} , coming from the columns of the AFt molecular structure can be seen. Figure 2.2b shows the bonds and locations of this ions. The hydrogen and hydroxyl bonds explained in subsection 3.2.5 can be observed at the high range of the spectra between 3200 and 3800 cm^{-1} and are marked in blue in figure 4.16. The results confirm the Raman spectroscopy observations of ettringite made in Black et al. (2006), Renaudin et al. (2007).

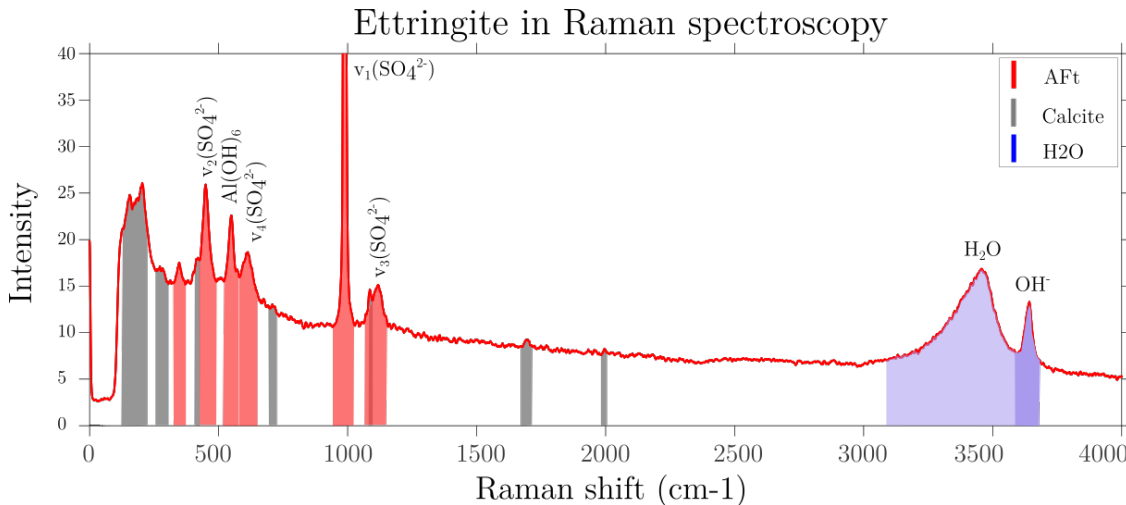


Figure 4.16: Raman shifts of ettringite without PCE. Calcite marked in grey, ettringite in red and blue.

Figure 4.17 compares the Raman spectra of the direct synthesized ettringite with (blue) and without (red) addition of 2% 3PMA1000. Ettringite with PCEs shows a higher calcite peaks (at 1074 , 268 and 301 cm^{-1}). Besides this, small and broad peaks can be seen at around 1460 as well as 2900 cm^{-1} , which are labelled "PCE Peak 1" and "PCE peak 2" in figure 4.17 and become more clear when looking at figure 4.18 that shows the Raman spectrum of the pure PCE. Moreover, no gypsum peaks can be observed, however it is possible that a small gypsum peak at 1009 cm^{-1} overlaps with the $v1$ sulphate vibration mode at 989 cm^{-1} . Furthermore, no shifts of the ettringite peaks could be observed between the AFt and AFt+PCE samples.

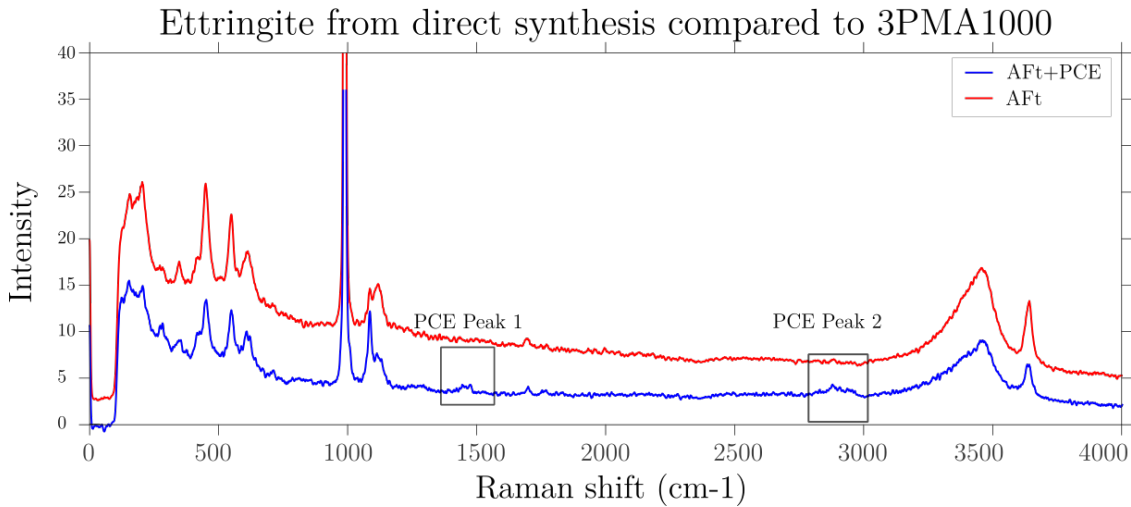


Figure 4.17: Raman shifts of ettringite with and without PCE (2% w/w of 3PMA1000). Besides a higher carbonation, the AFT+PCE sample show two small peaks at 1460 and 2900 cm^{-1} .

Figure 4.18 shows the Raman spectra of 3PMA1000 in black. The peaks coming from the PMA backbone are marked in dark blue, while bright blue marks the peaks from the PEG side chains (data from Koenig & Angood (1970), Corporation et al. (1969), Taylor (1973)). Comparing the "PCE Peak 1" and "PCE Peak 2" from the AFT+PCE spectra, it can be observed that they correlate with the main side chain and the main backbone peak of the PCE, respectively. Therefore PCE Peak 1 and 2 are now referred to as PCE Peak SC and PCE Peak BB.

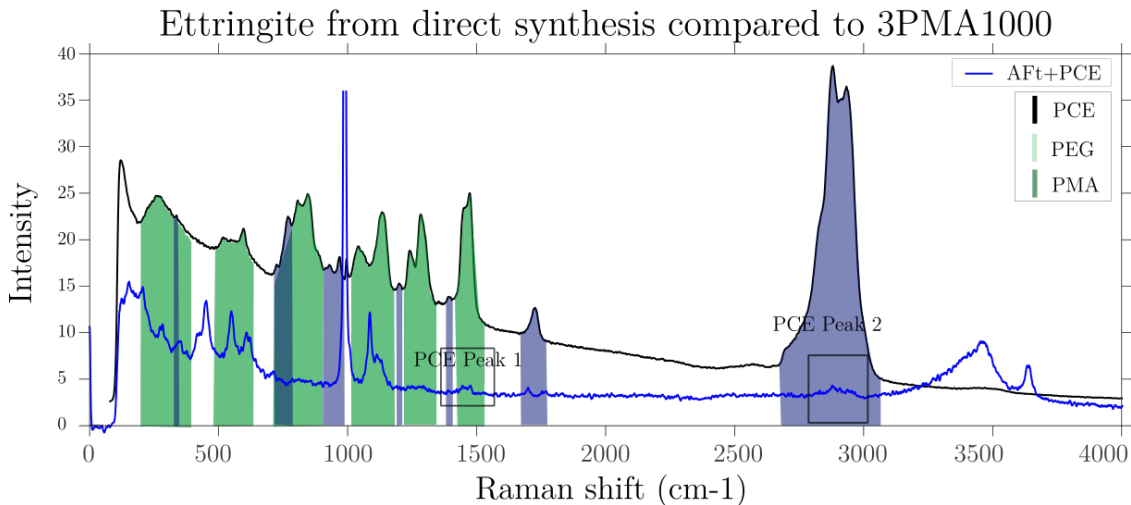


Figure 4.18: The AFT+PCE spectrum in blue is compared with the PCE spectrum in black. The different SC and BB peaks are marked in bright respectively dark green. The peaks from AFT+PCE that are not attributed with AFT or calcite, correlate with the biggest peaks of PCE. PCE peak 1 is attributed to the side chains, PCE peak 2 to the backbone.

The Raman results of ettringite from C_3A and hemihydrate reaction with and without 3PMA1000 can be seen in figure 4.19. The Raman spectra show less carbonation (as already observed by XRD) than ettringite from direct synthesis, but otherwise no difference can be seen. Both peaks coming from the PCE SC and BB can be observed. The deconvolution of the peaks is described in the next subsection.

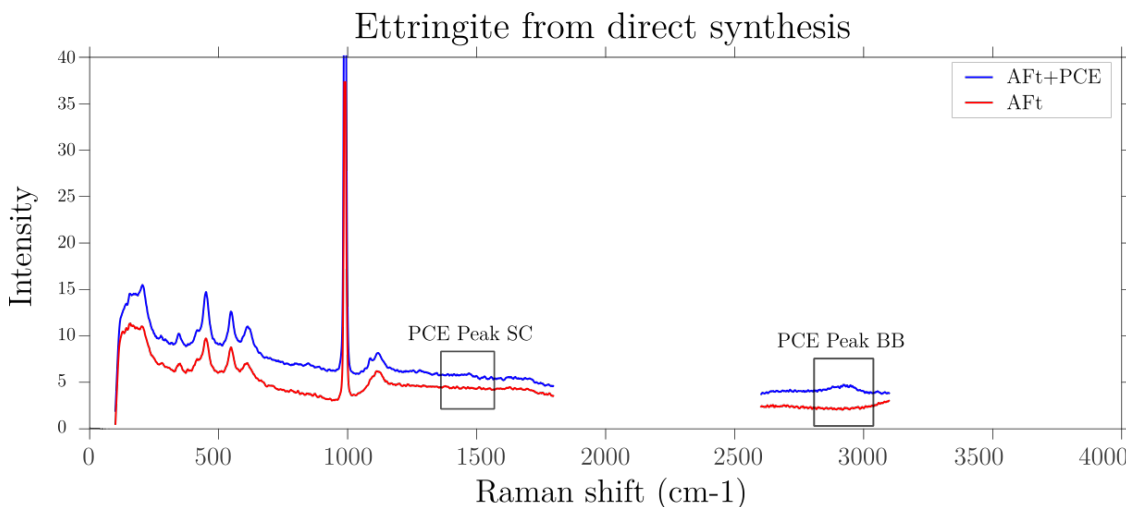


Figure 4.19: A reduced Raman spectra of ettringite with and without PCE of ettringite precipitated from C_3A and hemihydrate. The peaks correspond to the ones from 4.17

4.6.1 Deconvolution of PCE Peaks in Raman shifts of AFt+PCE

The left picture of figure 4.20 shows the side chain peak at 1460 cm^{-1} coming from the methylen group CH_2 present in the side chain. The same peak can be observed in the AFt+PCE sample from direct synthesis. Its deconvolution in the right pictures of figure 4.20 shows that this peak is not shifted in the ettringite sample. The "PCE peak SC" from the AFt+PCE sample made from C_3A reaction shows the same peak but is too small to be deconvoluted with precision.

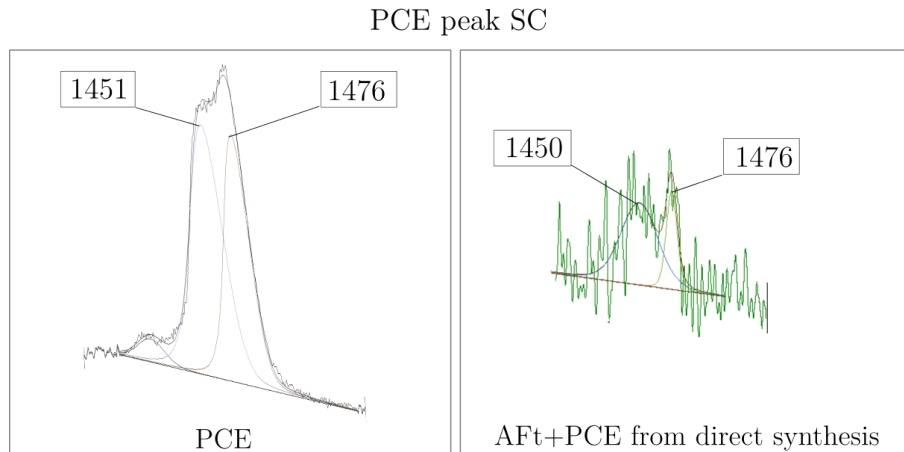


Figure 4.20: Raman shifts of ettringite with and without PCE as well as pure PCE between 1400 and 4000 cm^{-1}

Figure 4.21a shows the "PCE Peak BB" at 2900 cm^{-1} and compares the PCE, AFt and AFT+PCE spectra. The latter (in blue) shows a clear peak that correlates with the C-H bond of the PCE 3PMA1000 spectra (green). This peak can not be seen in any ettringite samples without PCE.

Figure 4.21b shows the deconvolution of the "PCE peak BB" at 2900 cm^{-1} . The picture in the middle shows the deconvolution of the 3PMA1000 peak. Six curves are used to get the best fit which indicates different vibrations of the atoms. The AFt+PCE spectra from the direct synthesis and the C_3A reaction is shown in the left and the right picture, respectively. When fitting the curve most peaks in both AFt+PCE spectra show a shift to the right. The left peak from the AFt+PCE samples (2820.7 and 2832.8 cm^{-1}) were compared to three peaks in same area for the PCE sample. This is why the peak-shift to the left, in the AFt+PCE sample from C_3A reaction (left pointed arrow in the left picture of figure 4.21b), could be an error of the curve fitting.

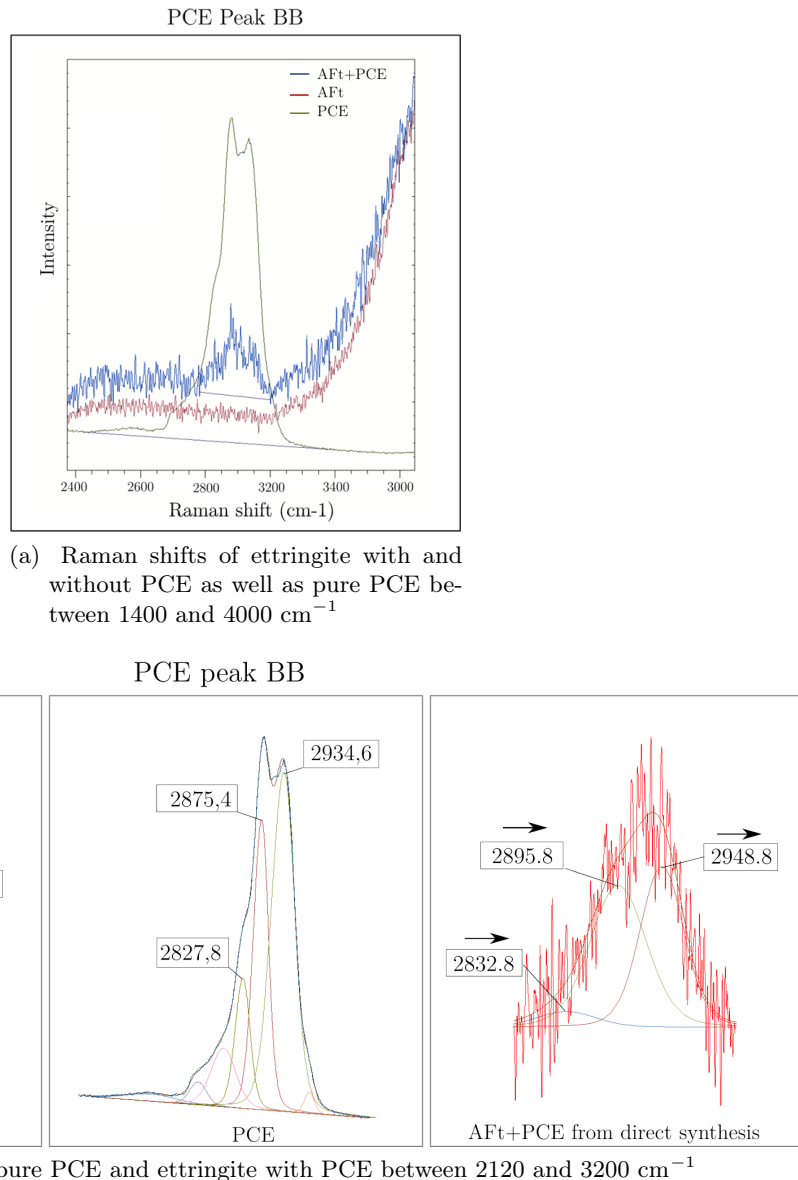


Figure 4.21: Deconvolution of "PCE peak BB" from Aft+PCE and PCE samples

5 Discussion

5.1 Morphology and formation of ettringite crystals

As mentioned in subsection 2.2.1, the morphology of ettringite can show different sizes and shapes depending on the environmental conditions, such as solution concentration and pH (Goetz-Neunhoeffer et al. (2006), Moore & Taylor (1970), Mantellato et al. (2016), Cody et al. (2004)).

In this studies, it was observed, that also PCEs have a big influence on the formation of ettringite crystals. For ettringite from direct synthesis, SEM images showed in samples without PCEs, around $2 \mu\text{m}$ long and $0.25 \mu\text{m}$ wide "barrel-shaped" short crystals and for ettringite with PCE addition (depending on the PCE dosage and molecular structure) up to $18 \mu\text{m}$ long and $0.15 \mu\text{m}$ wide fiber-like crystal needles. Some cases of PCE addition, however, showed the precipitation of shorter, "granular-like" ettringite crystals. This was also the case for ettringite from C_3A and hemihydrate reaction.

Furthermore results of the BET measurements confirm that PCE addition leads to a much higher SSA of ettringite crystals. It has been shown that the SSA for both, Aft and Aft+PCE samples, decreases over time, while maintaining an average ratio of 2.2 (figure 4.13).

All this information point to

- a strongly enhanced nucleation of ettringite in the first seconds to minutes (supporting the observations made by Dalas et al. (2015), Meier & Plank (2016), Cody et al. (2004)),
- a modification of crystal growth and
- a big influence of the heterogeneity of the solution.

The following two subsections show how PCE could modify the nucleation and growth of ettringite crystals. Afterwards the influence of the heterogeneity is discussed.

5.1.1 Nucleation

Figure 5.1 shows two hypotheses on how PCE could enhance the crystal nucleation of ettringite. The small dots label different kinds of ions in the solution whereas the grey blur spots represent nucleation areas. The PCE is illustrated by the FBW with the backbone and side chains. In the beginning (n1 and m1) the ions are well dispersed as assumed in the case of direct synthesis of ettringite.

In the first version (n1 to n4) the nucleation is enhanced by ions that accumulate in the

area around the PCEs. As a PCE molecule enters the well dispersed ion solution (n2), the positively charged aluminium and calcium ions get attracted by the negatively charged backbone. As PCEs are known to complex easily with such ions the negatively charged sulphate and hydroxyl ions than follow the Al and Ca ions. A double layer of ions could emerge similar to the DLVO theory (n3). The result is a locally increased supersaturation that leads to a higher nucleation rate (n4).

The other hypothesis (m1-m4) starts with a normal nucleation (m2). The PCEs then adsorb on this newly build formations and prevent further growth (m3). What follows is an increased nucleation at other places (m4). This theory was first suggested by [Cody et al. \(2004\)](#) and is supported by the results of [Meier et al. \(2016\)](#) that observed nano-sized long ettringite crystals precipitated after 10 seconds from a calcium hydroxide an aluminium sulphate solution.

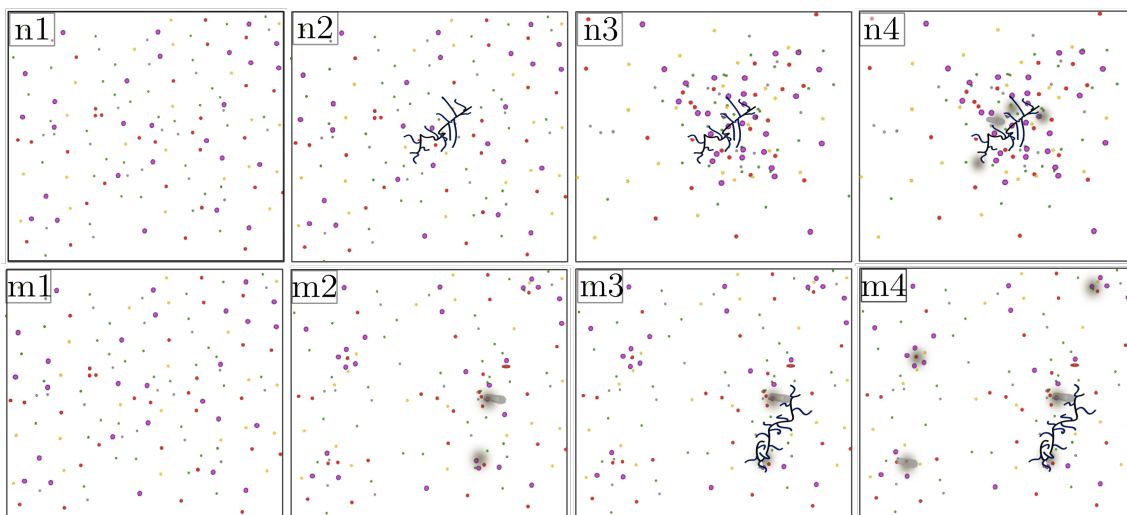


Figure 5.1: Hypotheses on how PCE could enhance the crystal nucleation of ettringite. n1 and m1 show homogeneously dispersed ions as assumed in the direct synthesis. In the first case (n2-n4) the PCE attracts ions and enhances nucleation by leading to a locally increased supersaturation. In the second case (m2-m4) PCE increase the nucleation indirectly by blocking the growth of freely formed nuclei through adsorption

Regarding hypothesis n, the crystal could develop around the polymer molecule. The fact that no d-spacing shifts could be observed by XRD measurements questions the presence of PCE in the material. Furthermore the obviously dispersed particles in the stirred solution with PCEs, would question the underlying working mechanism of PCEs (like steric hindrance) when they are trapped inside the crystals. Therefore the author suggests that the crystals form on the surface of the PCE.

5.1.2 Growth

Two mechanisms on how PCEs modify the crystal growth of ettringite once nuclei have formed are shown in figure 5.2.

In the first version (a1-a4) a high adsorption of PCEs on ettringite crystals (a2) inhibits their growth and forces an even higher nucleation rate that leads to smaller crystals, the size depending on the concentration of PCE (a3). This effect matches with the second nucleation version (m1-m4 in figure 5.1). The working mechanism has been suggested by [Cody et al. \(2004\)](#) and was supported by [Meier et al. \(2016\)](#) and [Dalas et al. \(2015\)](#). Moreover (in combination with the lower w/s ratio) this hypothesis might be the reason for the agglomeration of tiny crystals seen for ettringite with 15% PCE addition (a4). In the other case (b1-b4 in figure 5.1) the PCEs preferentially adsorb on the sides of the ettringite crystal (b2). As a result the crystals grow in length (b3). This way the long fiber-like ettringite crystals are created (b4) which have been observed in this study.

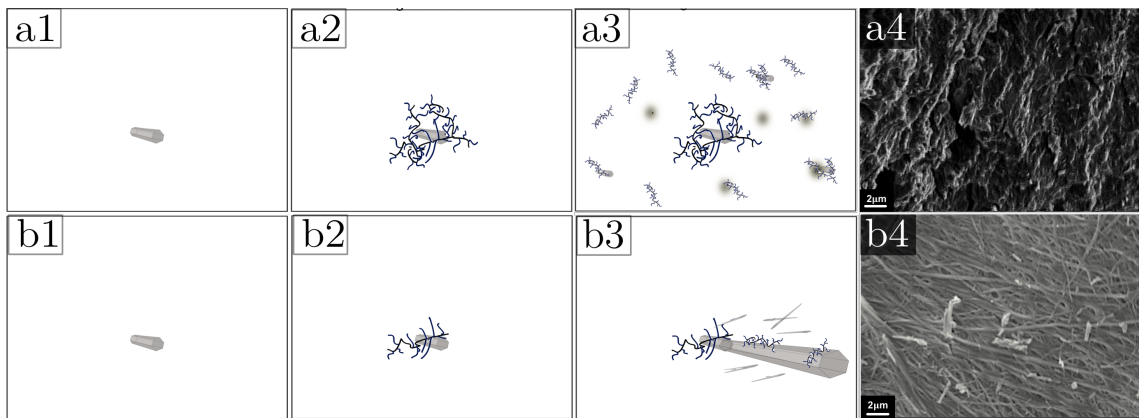


Figure 5.2: Two hypotheses on how PCEs modify crystal growth are shown. In the first version (a1-a3) the PCE inhibits growth completely leading to new nuclei and therefore more short crystals. In the second version only the growth in the a and b direction of ettringite is blocked.

5.1.3 Heterogeneity

The SEM pictures showed different formations of ettringite crystals. Either they precipitated as thin and long needles or as short and thicker hexagonal prisms. The author suggests that this is caused by the heterogeneity of the solution.

This hypothesis is supported by the fact that long-fiber like crystal needles were:

- always shown when prepared with the overhead stirrer and the flask

This could be caused by a better stirring quality and can be seen in figure 4.6).

- more often shown at higher PCE dosage

A better dispersion of crystals in the solution and place to grow.

- less evolved in ettringite from C_3A and hemihydrate reaction

The dissolution of C_3A leads to a heterogeneous system through the high ion

concentration close to the surface of the anhydrous phase. The precipitating ettringite crystals are very limited in space and therefore can not grow (see figure 4.10c). The adsorption of PCEs on anhydrous C_3A could lead to further disturbance.

- not shown in ettringite from C_3A and hemihydrate reaction, when a low w/s ratio was used.

The lower w/s ratio increases the space limitation of the ettringite precipitation. The result can be seen in figure 4.7 and 4.12b.

5.2 Influence of the PCE molecular structure on ettringite formation

The SEM image of figure 4.9 as well as the BET SSA results in figure 4.15a and 4.14 show the increased effectiveness coming from the higher charge density of 3PMA1000 compared to 3PMA3000. 3PMA1000 shows a stronger linear increase in SSA with PCE dosage than 3PMA3000. The same effect has been shown for the BET SSA results of [Dallas et al. \(2015\)](#).

When comparing the effect of the same amount of carboxylate group per gram of solid, the difference of the two polymers can still be seen. This leaves open questions on the workability of PCEs and possible scale factors.

5.3 Crystal structure of ettringite

The Raman spectroscopy results shows a change of state of the backbone between the polymer in solution (free) and the polymer on ettringite surface (adsorption state). The Raman shift of the peaks coming from the C-H bonds of the PMA in pure PCE and the AFt+PCE (figure 4.21b) indicate a modified bonding environment of PCEs when they are observed in ettringite. This modified bonding environment is most likely due to an interaction of those two materials. This would exclude that the Raman peaks result from not interacting PCEs that were not washed out during filtering.

None of the AFt peaks show any shifts. This would mean that the bonds of the ettringite structure are not modified or that a shift is not visible with Raman. The reason for the latter could lie in the dimension difference of the manipulated PCE bonds (PCE Peak BB) and the ettringite peaks. This theory is also supported by TGA results from pure 3PMA1000 that show a peak of the polymer that can not be seen in TGA measurements for AFt+PCE samples. A local change in crystal structure of ettringite can therefore not be seen by Raman spectroscopy.

6 Conclusion

In this study, it is shown that PCEs enhance the nucleation of ettringite crystals and disturb their growth from direct synthesis (i.e. reaction between dissolved CaO and $Al_2(SO_4)_3 \cdot 18H_2O$) as well as from C_3A and hemihydrate reaction.

- Ettringite from direct synthesis

Ettringite from direct synthesis without PCEs formed $2\mu m$ short and $0.25 \mu m$ wide ettringite crystals. A remarkable change in morphology was observed when PCEs were added into the solution. Ettringite precipitated as much as up to $18 \mu m$ long fiber-like crystal needles with a diameter of $0.15\mu m$.

Different hypotheses on the obvious interaction of PCEs on nucleation and growth were explained. One hypothesis is that nucleation and growth are modified through PCEs that adsorb on ettringite nuclei and crystals, respectively. The consequently inhibited (or strongly slowed down) nucleation and growth led to enhanced precipitation elsewhere in the solution. The strong increase in nucleation, however, could also be explained by a local concentration of ions attracted to the charged PCEs. Another hypothesis, which would explain the observed long, fiber-like needles from the direct synthesis, would be a restricted growth in width due to PCEs adsorbing onto the sides of ettringite crystals. A combination of those working mechanisms is likely to occur, depending on the ions and PCE concentration, the stirring volume and the geometry of the reactor used.

- Ettringite from reaction of C_3A with hemihydrate

Without PCE addition, no difference was found in the crystal morphology between the two synthesis methods. However, when PCE were added to the solution, an obvious influence on the morphology of the AFt crystals from the dissolution of C_3A was seen compared to the direct synthesis. Smaller, but not longer ettringite crystals precipitated.

The reason could be that the dissolving C_3A leads to a higher concentration of ions and therefore increased precipitation of ettringite crystals close to its surface. What follows is that it inhibits the ettringite crystals growth in length. PCEs that adsorb on the surface of C_3A could further influence the hydration kinetics.

Furthermore, it was observed that a lower w/s ratio leads to the precipitation of slightly thicker ettringite crystals. This could also be the result of an increased heterogeneity.

The Raman spectroscopy showed a change of backbone state in the polymer on the ettringite surface. However, the dimension of the PCE adsorbance is too small to see shifts in the ettringite peaks and thereby a change in crystal structure. The same goes for TGA measurements where the peak attributed to the degradation of polymer (400-450°C), couldn't be found in the ettringite samples with PCE.

BET gas adsorption measurements showed a linear increase of the SSA with added dosage of 3PMA3000 and 3PMA1000. Furthermore, the ratio of the SSA between the samples with and without PCE stayed constant, while the total SSA decreases with crystal growth over time.

7 Outlook

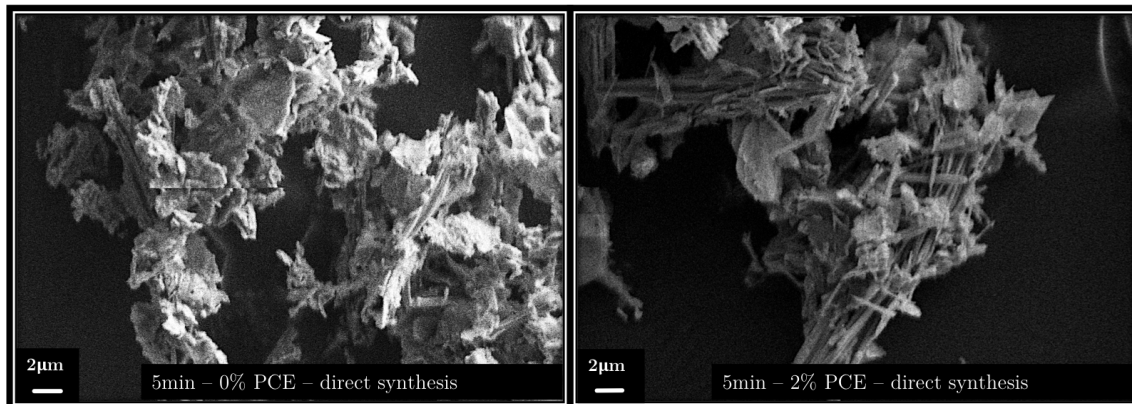
More work has to be done to further investigate the effect of PCEs on ettringite formation.

1. **BET SSA:** BET SSA measurements should be done on ettringite with different dosages of PCE with more molecular structure variation. This way the effect of the molecular structure of PCEs can be analysed, as well as the real dependence on the carboxylate contents.
2. **Time evolution:** Furthermore the ettringite formation during the first hour should be studied.

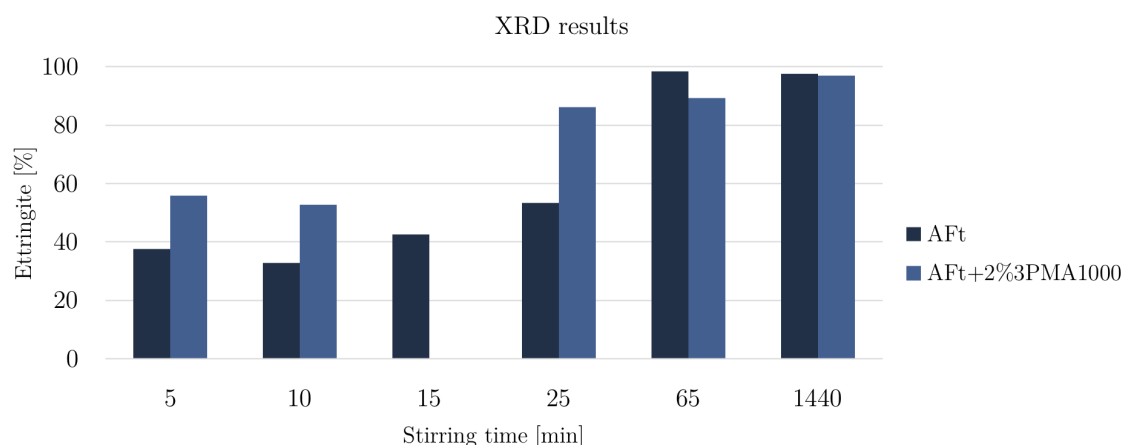
Preliminary tests have been performed to follow the evolution of ettringite crystals in the first hour. However, this could not be completely analysed within the scope of this work. Some of the preliminary results can be seen in figure 7.1a to 7.1b. One SEM image example of an ettringite sample stirred for 5 minutes with and without 2% (w/w) 3PMA1000 addition from direct synthesis can be seen in figure 7.1a. Figure 7.1b shows the XRD results of several samples during early hydration. The SEM images show very few smaller (left picture), or very long (right picture) ettringite crystal needles for no, or 2% (w/w) PCE addition, respectively. The XRD results in figure 7.1b reveal a relative amount of 37 respectively 45 % crystalline ettringite for the sample with and without PCE, the other phases being $CaCO_3$ and gypsum. Looking at the other XRD results, ettringite forms more quickly during the first 65 minutes. However, from the XRD patterns, the presence of an amorphous phase in the first hour was observed, which might change the relative quantity of ettringite in the system, when only analysing the crystalline phases by XRD. Therefore calculations using the external standard method were started to investigate the absolute weight fraction of stable ettringite in the system. However, the quantification method was not optimised with respect to the standard refinement. The results cannot be therefore fully trusted in an absolute way but the relative trend suggests less stable ettringite for system with PCEs (see appendix B).

When following the evolution of ettringite precipitation with PCEs in the first minutes/hour, there are important aspects that have to be mentioned: the adsorption of PCEs and the supersaturation degree of the solution. To do so, TOC (Total organic carbon) and ICP (inductively-coupled plasma mass spectrometry) measurements are needed.

3. **Particle size distribution:** Moreover the evolution of the particle size could be very informative and important for analysing the effect of PCEs on AFT precipitation. For early-age, small angle X-ray, scattering (SAXS) can be used. For later precipitation laser diffractometer also is possible.
4. **PCEs stability:** Additionally, the degradation of PCE in the alkaline solution could



(a) Comparing SEM images of ettringite from direct synthesis stirred for 5 min samples without and with 2% of 3PMA1000.



(b) XRD results for the samples with and without PCE addition during one hour of hydration, compared to the 24 hour (1440 min) stirred sample.

Figure 7.1: SEM and XRD results of ettringite samples with and without PCE, during early hydration.

be observed with the help of high-performance liquid chromatography (HPLC) or gel permeation chromatography (GPC).

3D printing and alternative cements

The understanding of the underlying mechanism and the quantification of the effects resulting from PCE addition is important for the development of new techniques in the construction industry, such as the development of printable 3-D concrete. In this application not only is the workability for concrete placing crucial, but also a high, early strength . As ettringite plays an important role in the rheological behaviour of concrete during the early ages and PCEs strongly affect its nucleation and growth, their interaction needs to be understood and controlled.

Furthermore, the working mechanism of PCE during early hydration is also important for an understanding of the increasing use of more environmental friendly alternative cements, using SCMs that have a high aluminium content. The observed, enhanced ettringite nucleation during the first few seconds could be very problematic, if not dramatic in practice, if not controlled.

Bibliography

- Aïtcin, P.-C. & Flatt, R. J. (2015), *Science and technology of concrete admixtures*, Woodhead Publishing.
- AMS (1992), ‘American Mineralogis Crystal Structure Database’.
URL: <http://rruff.geo.arizona.edu/AMS/amcsd.php>
- Baquerizo, L., Matschei, T. & Scrivener, K. (2016), ‘Impact of water activity on the stability of ettringite’, *Cem. Concr. Res.* **79**.
- Barger, G. S., Bayles, J., Blair, B., Brown, D., Chen, H., Conway, T. & Hawkins, P. (2001), ‘Ettringite Formation and the Performance of Concrete’, *Portl. Cem. Assoc.* (2166), 1–16.
- Behrens, G., Kuhn, L. T., Ubic, R. & Heuer, A. H. (1995), ‘Raman spectra of vateritic calcium carbonate’, *Spectrosc. Lett.* **28**(6), 983–995.
- Bittnar, Z., Bartos, P. J. M., Němeček, J., Šmilauer, V., Zeman, J., Jennings, H. M., Lee, J., Mahendra, S., Alvarez, P. J. J., Bartos, P. J. M., Scrivener, K., Ulm, F.-J., Vandamme, M., Constantinides, G., Smith, J. F., Decker, J. E., Bogdanov, A., Eves, B. J., Goodchild, D., Johnson, L., Kim, N., McDermott, M., Munoz-Paniagua, D., Pekelsky, J. R., Wingar, S., Zou, S. & et Al. (2009), Nanotechnology in Construction 3: Proceedings of the NICOM3, in ‘NICOM3’, p. 437.
URL: <http://dx.doi.org/10.1007/978-3-642-00980-8>
- Black, L., Breen, C., Yarwood, J., Deng, C.-S., Phipps, J. & Maitland, G. (2006), ‘Hydration of tricalcium aluminate (C3A) in the presence and absence of gypsum—studied by Raman spectroscopy and X-ray diffraction’, *J. Mater. Chem.* **16**(13), 1263.
URL: <http://xlink.rsc.org/?DOI=b509904h>
- Boeyens, J. C. A. & Ichharam, V. V. H. (2002), ‘Redetermination of the crystal structure of calcium sulphate dihydrate, Ca S O₄ * 2(H₂O).’, *Zeitschrift fuer Krist. - New Cryst. Struct.* **217**, 9–10.
- Brittain, R., Farmer, J. B., Jack, D., Martin, L. E. & Simpson, W. T. (1968), ‘© 1968 Nature Publishing Group’, *Nature* **219**(5156), 862–863.
- Christenson, H. K. (1984), ‘DLVO (Derjaguin-Landau-Verwey-Overbeek) theory and solvation forces between mica surfaces in polar and hydrogen-bonding liquids’, *J. Chem. Soc. Faraday Trans. 1* **80**(7), 1933–1946.
URL: <http://dx.doi.org/10.1039/F19848001933>
- Cody, A. M., Lee, H., Cody, R. D. & Spry, P. G. (2004), ‘The effects of chemical environment on the nucleation, growth, and stability of ettringite [Ca₃Al(OH)₆]₂(SO₄)₃·26H₂O’, *Cem. Concr. Res.* **34**(5), 869–881.

Compartet, C. (2004), Etude des interactions entre les phases modèles représentatives d'un ciment Portland et des superplastifiants du béton, PhD thesis.

URL: <http://www.theses.fr/2004DIJOS051>

Compartet, C., Pourchet, S., Nonat, A. & Maitrasse, P. (2007), 'Influence of Three Types of Superplasticizers on Tricalcium Aluminate Hydration in Presence of Gypsum.', *12th Int. Congr. Chem. Cem. Montr. Canada* pp. 3–3.

Corporation, T. P.-e., Tobin, M. C., Testes, S., Acid, D. & Baak, T. (1969), 'Laser Raman Spectra of Polymetbacrylic Acid', *Chem. Phys.* **50**(10), 4551–4554.

Dalas, F., Pourchet, S., Rinaldi, D., Nonat, A., Sabio, S. & Mosquet, M. (2015), 'Modification of the rate of formation and surface area of ettringite by polycarboxylate ether superplasticizers during early C3A-CaSO₄hydration', *Cem. Concr. Res.* **69**, 105–113.

URL: <http://dx.doi.org/10.1016/j.cemconres.2014.12.007>

De La Pierre, M., Carteret, C., Maschio, L., André, E., Orlando, R. & Dovesi, R. (2014), 'The Raman spectrum of CaCO₃ polymorphs calcite and aragonite: A combined experimental and computational study', *J. Chem. Phys.* **140**(16), 164509.

Eusebio, L., Goisis, M., Manganelli, G., Paternò, V. A. & Gronchi, P. (2013), 'Influence of Comb-Polymer Structure on C₃S₁ Phase Hydration', *Mater. Sci. Appl.* **04**(12), 35–44.

URL: <http://www.scirp.org/journal/doi.aspx?DOI=10.4236/msa.2013.412A006>

Flatt, R. J., Schober, I., Raphael, E., Plassard, C. & Lesniewska, E. (2009), 'Conformation of adsorbed comb copolymer dispersants', *Langmuir* **25**(2), 845–855.

Garrault, S., Behr, T. & Nonat, A. (2006), 'Formation of the C-S-H layer during early hydration of tricalcium silicate grains with different sizes', *J. Phys. Chem. B* **110**(1), 270–275.

Gay, C. & Raphaël, E. (2001), 'Comb-like polymers inside nanoscale pores', *Adv. Colloid Interface Sci.* **94**(1-3), 229–236.

Gelardi, G. & Flatt, R. J. (2015), *Working mechanisms of water reducers and superplasticizers*, Vol. 2, Elsevier Ltd.

URL: <http://dx.doi.org/10.1016/B978-0-08-100693-1.00011-4>

Gelardi, G., Mantellato, S., Marchon, D., Palacios, M., Eberhardt, A. B. & Flatt, R. J. (2015), *Chemistry of chemical admixtures*, Elsevier Ltd.

URL: <http://dx.doi.org/10.1016/B978-0-08-100693-1.00009-6>

Goetz-Neunhoeffer, F., Neubauer, J. & Schwesig, P. (2006), 'Mineralogical characteristics of Ettringites synthesized from solutions and suspensions', *Cem. Concr. Res.* **36**(1), 65–70.

Goto, S., Suenaga, K., Kado, T. & Fukuhara, M. (1995), 'Calcium Silicate Carbonation Products'.

Graf, D. L. (1961), 'Crystallographic tables for the rhombohedral carbonates', *Am. Mineral.* **46**, 1283–1316.

Hartman, M. R. & Berliner, R. (2006), 'Investigation of the structure of ettringite by time-of-flight neutron powder diffraction techniques', *Cem. Concr. Res.* **36**(2), 364–370.

- HOLZER, L., GASSER, P., KAECH, A., WEGMANN, M., ZINGG, A., WEPF, R. & MUENCH, B. (2007), 'Cryo-FIB-nanotomography for quantitative analysis of particle structures in cement suspensions', *J. Microsc.* **227**(3), 216–228.
URL: <http://doi.wiley.com/10.1111/j.1365-2818.2007.01804.x>
- Huang, H., Qian, C., Zhao, F., Qu, J., Guo, J. & Danzinger, M. (2016), 'Improvement on microstructure of concrete by polycarboxylate superplasticizer (PCE) and its influence on durability of concrete', *Constr. Build. Mater.* **110**, 293–299.
URL: <http://dx.doi.org/10.1016/j.conbuildmat.2016.02.041>
- Jansen, D., Neubauer, J., Goetz-Neunhoeffer, F., Haerzschen, R. & Hergeth, W.-D. (2012), 'Change in reaction kinetics of a Portland cement caused by a superplasticizer — Calculation of heat flow curves from XRD data', *Cem. Concr. Res.* **42**(2), 327–332.
URL: <https://www.sciencedirect.com/science/article/pii/S0008884611002699>
- Koenig, L. & Angood, A. C. (1970), 'Spectra of Poly(ethylene Glycols) in Solution', *J. Polym. Sci.* **1796**, 1787–1796.
- Lasaga, A. & L\"uttge, A. (2001), 'Variation of Crystal Dissolution Rate Based on a Dissolution Step Wave Model', *Science (80-.).* **291**(March), 2400–2404.
- Li, Y., Yang, C., Zhang, Y., Zheng, J., Guo, H. & Lu, M. (2014), 'Study on dispersion, adsorption and flow retaining behaviors of cement mortars with TPEG-type polyether kind polycarboxylate superplasticizers', *Constr. Build. Mater.* **64**, 324–332.
URL: <https://www.sciencedirect.com/science/article/pii/S0950061814003675?via%3Dihub>
- Mantellato, S., Palacios, M. & Flatt, R. J. (2016), 'Impact of sample preparation on the specific surface area of synthetic ettringite', *Cem. Concr. Res.* **86**, 20–28.
- Marchon, D. (2016), 'Controlling Cement Hydration Through the Molecular Structure of Comb Copolymer Superplasticizers', p. 215.
URL: <http://e-collection.library.ethz.ch/eserv/eth:50178/eth-50178-02.pdf>
- Marchon, D. & Flatt, R. J. (2016), *8 - Mechanisms of cement hydration*, Elsevier Ltd.
URL: <http://dx.doi.org/10.1016/B978-0-08-100693-1.00008-4>
- Marchon, D., Juillard, P., Gallucci, E., Frunz, L. & Flatt, R. J. (2017), 'Molecular and submolecular scale effects of comb-copolymers on tri-calcium silicate reactivity : Toward molecular design', (November 2016), 817–841.
- Marchon, D., Mantellato, S., Eberhardt, A. & Flatt, R. (2016), *Adsorption of chemical admixtures*, Elsevier Ltd.
URL: <http://linkinghub.elsevier.com/retrieve/pii/B9780081006931000102>
- Material, S. R. (2012), 'Certificate of Analysis; SRM 1898 - Titanium Dioxide Nanomaterial', *Nist* (June), 1–16.
URL: <https://www-s.nist.gov/srmors/certificates/1898.pdf>
- Mehta, P. K. & Monteiro, P. J. M. (1976), 'Concrete: microstructure, properties, and materials. 2006', *Util. palm oil fuel ash Concr. a Rev. .*
- Meier, M. R. & Plank, J. (2016), 'Crystal growth of $[Ca_3Al(OH)_6 \cdot 12H_2O]_2 \cdot (SO_4)_3 \cdot 2H_2O$ (ettringite) under microgravity: On the impact of anionicity of polycarboxylate comb polymers', *J. Cryst. Growth* **446**, 92–102.
URL: <http://dx.doi.org/10.1016/j.jcrysgro.2016.04.049>

- Meier, M. R., Rinkenburger, A. & Plank, J. (2016), 'Impact of different types of polycarboxylate superplasticisers on spontaneous crystallisation of ettringite', *Adv. Cem. Res.* **28**(5), 310–319.
URL: <http://www.icevirtuallibrary.com/doi/10.1680/jadcr.15.00114>
- Micaela, D. R. (2015), 'Highlights in Mineralogical Crystallography'.
URL: <https://www.degruyter.com/view/product/455037>
- Moore, A. E. & Taylor, H. F. W. (1970), 'Crystal structure of ettringite', *Acta Crystallogr. Sect. B Struct. Crystallogr. Cryst. Chem.* **26**(4), 386–393.
URL: <http://scripts.iucr.org/cgi-bin/paper?S0567740870002443>
- Pustovgar, E., Mishra, R. K., Palacios, M., d'Espinose de Lacaillerie, J. B., Matschei, T., Andreev, A. S., Heinz, H., Verel, R. & Flatt, R. J. (2017), 'Influence of aluminates on the hydration kinetics of tricalcium silicate', *Cem. Concr. Res.* **100**(April), 245–262.
URL: <https://doi.org/10.1016/j.cemconres.2017.06.006>
- Regnaud, L., Rossina, C., Alfani, R. & Vichot, a. (2011), Effect of Comb type Superplasticizers on hydration kinetics of Industrial Portland cements, in '13th Int. Congr. Chem. Cem.', Vol. 33, pp. 1–7.
- Renaudin, G., Segni, R., Mentel, D., Nedelev, J.-M., Leroux, F. & Taviot-Gueho, C. (2007), 'A Raman Study of the Sulfated Cement Hydrates: Ettringite and Monosulfoaluminate', *J. Adv. Concr. Technol.* **5**(3), 299–312.
- Roessler, C., Moeser, B. & Stark, J. (2007), Influence of Superplasticizers on C 3 A Hydration and Ettringite Growth in Cement Paste, in '12th Int. Congr. Chem. Cem.'
- Schofield, P. F., Knight, K. S. & Stretton, I. C. (1996), 'Thermal expansion of gypsum investigated by neutron powder diffraction T = 320 K', *Am. Mineral.* **81**, 847–851.
- Scrivener, K., Snellings, R. & Lothenbach, B. (2016), *A Practical Guide to Microstructural Analysis of Cementitious Materials*.
- Sitepu, H., O'Connor, B. H. & Li, D. (2005), 'Comparative evaluation of the March and generalized spherical harmonic preferred orientation models using X-ray diffraction data for molybdate and calcite powders', *J. Appl. Crystallogr.* **38**(1), 158–167.
- Taylor, P. (1973), 'Conformational Studies of Poly [methacrylic Acid]. II . laser-Excited Raman Studies of the Conformational Transition in Aqueous Solution *', *J. Am. Chem. Soc.* **95**(23), 7866–7872.
- Wiliński, D., Łukowski, P. & Rokicki, G. (2016), 'Polymeric superplasticizers based on polycarboxylates for ready-mixed concrete: Current state of the art', *Polimery/Polymers* **61**(7-8), 474–481.
- Winnefeld, F., Zingg, A., Holzer, L., Figi, R., Pakusch, J. & Becker, S. (2007), 'Interaction of Polycarboxylate-based Superplasticizers and Cements: Influence of Polymer Structure and C3A-content of Cement', *12th Int. Congr. Chem. Cem.* pp. 1–12.
- Wu, H., Guo, H., Lei, J., Zhang, R. & Liu, Y. (2007), 'Research on synthesis and action mechanism of polycarboxylate superplasticizer', *Front. Chem. China* **2**(3), 322–325.
URL: <https://doi.org/10.1007/s11458-007-0060-2>

- Yamada, K. (1992), 'A Summary of Important Characteristics of Cement and Superplasticizers', *Spec. Publ.* **262**.
- Zhang, J. & Scherer, G. W. (2011), 'Comparison of methods for arresting hydration of cement', *Cem. Concr. Res.* **41**(10), 1024–1036.
URL: <http://dx.doi.org/10.1016/j.cemconres.2011.06.003>
- Zhang, L. & Glasser, F. P. (2000), 'Critical examination of drying damage to cement pastes', *Adv. Cem. Res.* **12**(2), 79–88.
URL: <https://doi.org/10.1680/adcr.2000.12.2.79>
- Zhang, Y.-R., Kong, X.-M., Lu, Z.-B., Lu, Z.-C. & Hou, S.-S. (2015), 'Effects of the charge characteristics of polycarboxylate superplasticizers on the adsorption and the retardation in cement pastes', *Cem. Concr. Res.* **67**, 184–196.
URL: <https://www.sciencedirect.com/science/article/pii/S0008884614001987>
- Zhang, Z., Scherer, G. W. & Bauer, A. (2018), 'Morphology of cementitious material during early hydration', *Cem. Concr. Res.* **107**(February), 85–100.
URL: <https://doi.org/10.1016/j.cemconres.2018.02.004>
- Zingg, A., Holzer, L., Kaech, A., Winnefeld, F., Pakusch, J., Becker, S. & Gauckler, L. (2008a), 'The microstructure of dispersed and non-dispersed fresh cement pastes - New insight by cryo-microscopy', *Cem. Concr. Res.* **38**(4), 522–529.
- Zingg, A., Holzer, L., Kaech, A., Winnefeld, F., Pakusch, J., Becker, S. & Gauckler, L. (2008b), 'The microstructure of dispersed and non-dispersed fresh cement pastes — New insight by cryo-microscopy', *Cem. Concr. Res.* **38**(4), 522–529.
URL: <https://www.sciencedirect.com/science/article/pii/S0008884607002906?via%3Dihub>
- Zingg, A., Winnefeld, F., Holzer, L., Pakusch, J., Becker, S., Figi, R. & Gauckler, L. (2009), 'Interaction of polycarboxylate-based superplasticizers with cements containing different C3A amounts', *Cem. Concr. Compos.* **31**(3), 153–162.

A Sample specifications

[g]	Reference	II	II (Al6504B-18)	H ₂ O)	+ (CaO	I (stirring for 1h) + H ₂ O)	PCE solution	II	%PCE/s	Amount [g]	Stirring type
16.11	1.068	33.320	+	0.538	466.766	+		->	~2	24h	0
17.11	1.066	33.333	+	0.539	466.667	+		->	~2	4h	0
20.11_Ns28	1.066	33.338	+	0.538	466.559	+	0.138	->	~2	24h	~2
21.11_Ns28	1.065	33.325	+	0.538	466.550	+	0.128	->	~2	4h	~2
6.12_1_Ns28	1.066	33.328	+	0.537	466.543	+	0.134	->	~2	7d	~2
6.12_11	1.066	33.340	+	0.538	466.661	+		->	~2	7d	0
13.17_1_Ns28	1.065	33.348	+	0.538	466.576	+	0.130	->	~2	54h	~2
13.17_11	1.065	33.339	+	0.538	466.672	+		->	~2	54h	0
16.12_1_Ns32	0.640	+	20.020	+	0.320	+	280.010	+	~0.047	24h	~1.9
16.12_11_Ns32	0.640	+	20.050	+	0.330	+	279.930	+	0.019	~24h	~0.81
17.12_1_Ns28	0.640	+	20.002	+	0.323	+	280.003	+	0.020	~24h	~0.5
17.12_11_Ns32	0.639	+	20.031	+	0.324	+	279.880	+	0.188	~24h	~7.56
17.12_111_Ns32	0.640	+	20.040	+	0.322	+	280.608	+	0.081	~24h	~3.24
24.1_1_Ns28	0.639	+	20.021	+	0.322	+	279.933	+	0.080	~24h	~2
24.1_11_F_Ns28	0.639	+	20.073	+	0.322	+	279.933	+	0.080	~24h	~2
25.1_1_Ns28	4.301	+	5.400	+	2.171	+	95.088	+	4.062	~24h	~15
31.1_1	1.065	33.339	+	0.537	466.674	+		->	~2	5.10.15.25.4	0
31.1_11_Ns28	1.065	33.338	+	0.537	466.679	+	0.134	->	~2	5.10.15.25.4	~3.24
5.2_1_FN"	0.640	20.000	+	0.322	279.929	+	0.081	->	~1.2	24h	~3.24
7.2_1_Ns28	0.640	+	20.010	+	0.323	+	279.940	+	0.083	~24h	~2
7.2_11	6.400	+	20.108	+	0.323	+	280.040	+		~24h	0

h... Hours m ... Magnetic
d... Days F ... Flask
others minutes N ... Nitrogen

Figure A.1: Summary of all samples prepared in the scope of this work. Starting with a reference name the table shows the stoichiometric composition of the raw materials in gram. Afterwards information on the stirring time, percentage of PCEs of solid content, total amount of synthesized ettringite as well as stirring type is given

B External Standard

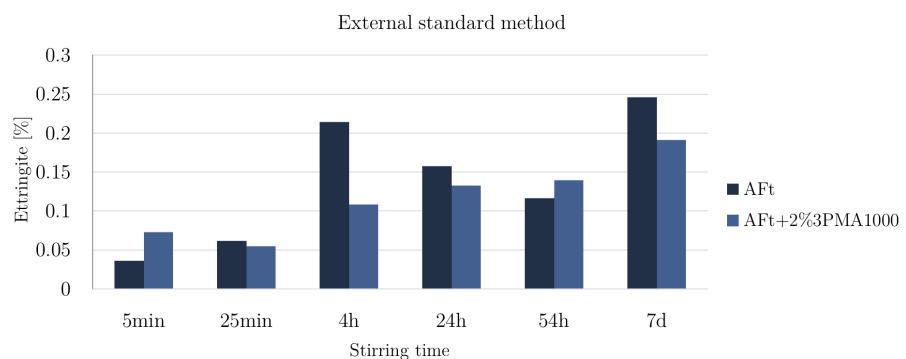


Figure B.1: Preliminary results from the external standard method for selected samples.